*remote sensing*

MDPI

*Article*

# Mapping the Leaf Economic Spectrum across West African Tropical Forests Using UAV-Acquired Hyperspectral Imagery

**Eleanor R. Thomson [1,2,*], Yadvinder Malhi [1], Harm Bartholomeus [3], Imma Oliveras [1], Agne Gvozdevaite [1], Theresa Peprah [4], Juha Suomalainen [3,5], John Quansah [4], John Seidu [4], Christian Adonteng [4], Andrew J. Abraham [2], Martin Herold [3], Stephen Adu-Bredu [4] and Christopher E. Doughty [2]**

1 Environmental Change Institute, School of Geography and the Environment, University of Oxford, Oxford OX1 3QY, UK; yadvinder.malhi@ouce.ox.ac.uk (Y.M.); imma.OLIVERAS@ouce.ox.ac.uk (I.O.); agne.gvozdevaite@kellogg.ox.ac.uk (A.G.)

2 School of Informatics, Computing, and Cyber Systems, Northern Arizona University, Flagstaff, AZ 86011, USA; andrew.abraham@nau.edu (A.J.A.); chris.doughty@nau.edu (C.E.D.)

3 Laboratory of Geo-Information Science and Remote Sensing, Wageningen University, P.O. Box 47, 6700 AA Wageningen, The Netherlands; harm.bartholomeus@wur.nl (H.B.); juha.suomalainen@nls.fi (J.S.); martin.herold@wur.nl (M.H.)

4 Forestry Research Institute of Ghana, Council for Scientific and Industrial Research, P.O. Box UP 63 KNUST, Kumasi, Ghana; tpeprah@csir-forig.org.gh (T.P.); johnquansah18@gmail.com (J.Q.); johnseidu@gmail.com (J.S.); adonboaheng2@gmail.com (C.A.); sabredu@gmail.com (S.A.-B.)

5 Finnish Geospatial Research Institute, National Land Survey of Finland, Geodeetinrinne 2, 02430 Masala, Finland

* Correspondence: eleanor.thomson@oriel.ox.ac.uk; Tel.: + 44-7305-983-877

Received: 15 August 2018; Accepted: 13 September 2018; Published: 24 September 2018


**Abstract:** The leaf economic spectrum (LES) describes a set of universal trade-offs between leaf mass per area (LMA), leaf nitrogen (N), leaf phosphorus (P) and leaf photosynthesis that influence patterns of primary productivity and nutrient cycling. Many questions regarding vegetation-climate feedbacks can be addressed with a better understanding of LES traits and their controls. Remote sensing offers enormous potential for generating large-scale LES trait data. Yet so far, canopy studies have been limited to imaging spectrometers onboard aircraft, which are rare, expensive to deploy and lack fine-scale resolution. In this study, we measured VNIR (visible-near infrared (400–1050 nm)) reflectance of individual sun and shade leaves in 7 one-ha tropical forest plots located along a 1200–2000 mm precipitation gradient in West Africa. We collected hyperspectral imaging data from 3 of the 7 plots, using an octocopter-based unmanned aerial vehicle (UAV), mounted with a hyperspectral mapping system (450–950 nm, 9 nm FWHM). Using partial least squares regression (PLSR), we found that the spectra of individual sun leaves demonstrated significant ($p < 0.01$) correlations with LMA and leaf chemical traits: $r^2 = 0.42$ (LMA), $r^2 = 0.43$ (N), $r^2 = 0.21$ (P), $r^2 = 0.20$ (leaf potassium (K)), $r^2 = 0.23$ (leaf calcium (Ca)) and $r^2 = 0.14$ (leaf magnesium (Mg)). Shade leaf spectra displayed stronger relationships with all leaf traits. At the airborne level, four of the six leaf traits demonstrated weak ($p < 0.10$) correlations with the UAV-collected spectra of 58 tree crowns: $r^2 = 0.25$ (LMA), $r^2 = 0.22$ (N), $r^2 = 0.22$ (P), and $r^2 = 0.25$ (Ca). From the airborne imaging data, we used LMA, N and P values to map the LES across the three plots, revealing precipitation and substrate as co-dominant drivers of trait distributions and relationships. Positive N-P correlations and LMA-P anticorrelations followed typical LES theory, but we found no classic trade-offs between LMA and N. Overall, this study demonstrates the application of UAVs to generating LES information and advancing the study and monitoring tropical forest functional diversity.

**Keywords:** leaf traits; leaf economic spectrum; UAV; hyperspectral; spectroscopy; tropical forest; PLSR; Ghana; West Africa

## 1. Introduction

Plant functional traits refer to specific features about a plant's morphological and physiological characteristics that determine factors such as its preferred environment, growth rate, life strategy, dispersal ability and tolerance of pests and hazards [1]. As plant traits tend to represent fundamental trade-offs that determine a species' ecological performance, there is currently much interest in using plant traits to link species richness to functional diversity to better understand the influence of biological communities on ecosystem function [2–6] and improve predictions of ecosystem response to environmental change [7–9].

Leaf traits demonstrate a direct link to ecosystem function via the Leaf Economic Spectrum (LES). The LES describes an axis of six main leaf traits (leaf mass per area (LMA), leaf nitrogen (N), leaf phosphorus (P), leaf longevity, photosynthetic rate, and dark respiration rate) that covary in predictable ways and underpin plant resource acquisition–defence tradeoffs [10,11]. On one end of the spectrum, species opt for a quick return on investments by producing 'cheap', short-lived leaves with high N and P concentrations that facilitate high photosynthesis rates and fast growth. These species are commonly found in high-fertility environments where short lived leaves from abscission and herbivory maintain relatively fast rates of nutrient cycling [12,13]. On the other end of the spectrum, species located in lower-precipitation and -nutrient regimes tend to trade rapid growth for persistence and invest in tough, well-protected leaves, with higher LMA values and lower N and P concentrations. They produce leaves that can better withstand herbivory and physical hazards, leading to increased leaf longevity and a lower rate of nutrient cycling [14,15]. The LES has been shown to be a good indicator of plant performance [16,17], with a species' position on the spectrum describing the plant's overall strategy (quick growing but ephemeral versus slow growing but enduring). Importantly, this spectrum has been shown to operate similarly across a wide variety of species and biomes, with important implications for global dynamic vegetation and climate models [18].

Despite the fact that functional traits have been found to form the basis of a more quantitative and predictive ecology, a major limitation to this research has been a lack of spatially extensive trait data [19]. This lack of trait data is particularly severe in tropical forests [20]. Tall trees, high species diversity and the labour-intensive nature of collecting trait data, combined with the inaccessibility of many tropical regions, means measuring and monitoring functional traits in tropical areas is a time-consuming and expensive process. Yet tropical forests comprise 40–50% of the total carbon in terrestrial vegetation [21–23], store a third of global soil carbon [24] and currently absorb around 18% of human $CO_2$ emissions [25]. Thus, determining the functional diversity of tropical forest canopies is critical to predicting future climate–biosphere interactions, as a small perturbation in the net balance of tropical forest carbon cycling would have significant climate implications.

Remote sensing offers enormous potential for generating large-scale trait data. Using high-resolution spectroscopy (VNIR (400–1100) or VSWIR (400–2500 nm)) to measure plant foliar traits has a long scientific record [26,27]. Specific spectral absorption features have been directly linked to a leaf's concentration of cellulose, lignin, chlorophylls, N, starch, oil, proteins and water (see Curran [28] for a well-known synthesis). For example, the measurement of N, bound in chlorophyll and proteins, is associated with the bandwidths between 460–480, 650–670 and 1510–1600 nm [29,30], while LMA can be indirectly estimated using variations in leaf thickness and leaf water content expressed across the 700–1300 nm range [31–33].

In the last decade, significant headway has been made in the remote sensing of tropical forest leaf traits, both at the individual leaf level and at the canopy level [34]. Relationships between spectra and foliar traits have been developed using partial least squares regression analysis (PLSR). The PLSR

technique is useful because it does not focus on a small number of wavelengths but uses the entire leaf spectral continuum in its analysis. It is designed to handle situations where the number of predictor variables (e.g., 101 spectral bands) is higher than the number of observations, avoiding earlier problems of collinearity and statistical overfitting [35,36]. Using PLSR, relationships have also been found between leaf spectra and macronutrients, such as P, K, Ca and Mg, that have no direct expression in the VNIR or VSWIR, but often demonstrate correlations with other traits [20,37–40].

Similarly, using PLSR and spectroscopy, it has been found that 'higher-order' foliar traits, such as photosynthesis and respiration, can be predicted with a high degree of accuracy and precision [33]. Globally, the largest fraction of net primary productivity (NPP: 30–40%) is thought to occur in tropical forests [41–43]. Yet there are fears that, in the Amazon at least, this value may be decreasing [44]. Satellite-based techniques for measuring tropical NPP have attracted recent criticism, as they demonstrate little spatial or temporal agreement with plot-based values [45]. Thus, UAV-based spectroscopy may offer a new approach for estimating NPP across small-scale tropical forest areas.

This paper aims to investigate the use of UAVs for the mapping and monitoring of tropical forest canopy traits. Using a similar method to leaf spectroscopy, airborne hyperspectral imaging spectrometers measure solar radiation REFLECTED from the forest canopy at numerous narrow wavelengths, producing estimates of canopy foliar traits at scales unachievable via field and lab approaches [46–48]. In the last ten years, developments and improvements in UAVs, together with the miniaturization of sensing technologies, has opened up previously unavailable opportunities for remote sensing. In comparison to aircraft, UAVs are accessible to a wide array of researchers, they can operate at short notice without a planned schedule, and provide high spatial and spectral resolution data at low cost. Although their flight duration is much shorter than that of an aircraft, limiting their area of data collection, they can fly slower, at much lower altitudes, and thus acquire higher spatial and temporal resolution data [49]. Using UAVs to map and monitor tropical forest canopy traits would have distinct advantages over aircraft in that they would (i) enable a wider proportion of the research community to quantify canopy traits, increasing spatial coverage and innovation in this area, (ii) facilitate the swift upscaling of field study results to the immediate geographic area, (iii) be able to be deployed quickly after a disturbance event, such as a drought or fire, to measure its effects, (iv) be able to be deployed on multiple occasions over a short time period to monitor temporal changes, and (v) assist in a wide range of conservation related projects and programmes and promote an interest in plant traits outside of the academic community [50,51].

Using data collected across a tropical forest precipitation gradient in West Africa, this study seeks to answer the following questions:

(i) Can high-resolution VNIR spectroscopy predict LMA, N, P, K, Ca and Mg in sun and shade leaves at the individual leaf level? While sun leaves have received a lot of attention in remote sensing studies due to their natural prominence in airborne imaging data, shade leaves (those located under the canopy in the understory) constitute the majority of tropical forest foliage and are known to have a strong influence on canopy spectral signatures in the near-infrared (NIR).
(ii) Can the same foliar traits be quantified with similar accuracy and precision at the tree crown level using UAV-collected hyperspectral imagery?
(iii) Can UAV-collected hyperspectral imagery be used to map these leaf traits across forest plots?
(iv) Does the spatial distribution of traits and their relationships subscribe to general LES theory?

## 2. Materials and Methods

### *2.1. The Study Sites*

Data collection was carried out at three sites across a precipitation gradient in Ghana: Ankasa Conservation Area, Bobiri Forest Reserve and Kogyae Strict Nature Reserve (Figure 1). The three study sites form part of the Global Ecosystems Monitoring network (GEM: gem.tropicalforests.ox.ac.uk), which is a long-term effort to measure and monitor forests and their response to climate change.

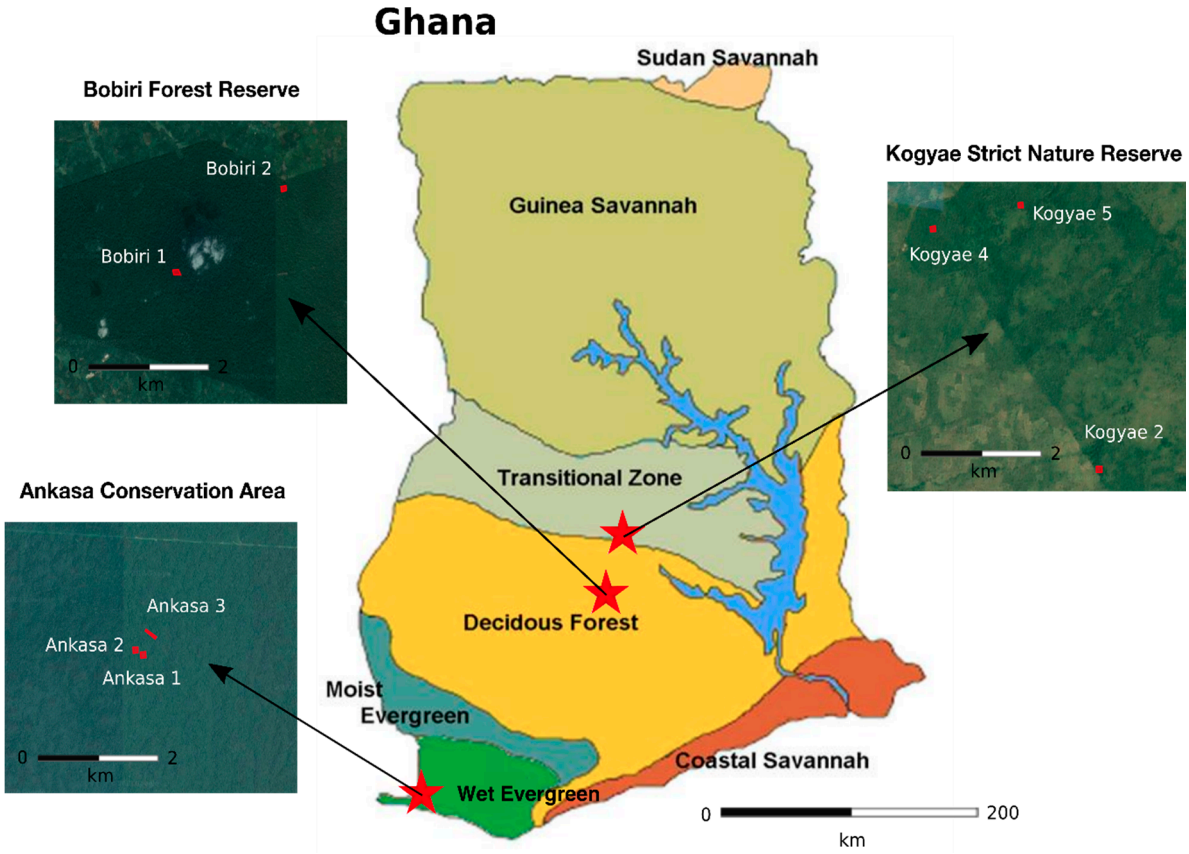


**Figure 1.** Map showing the major ecological zones of Ghana and location of research sites (Ankasa Conservation Area, Bobiri Forest Reserve and the Kogyae Strict Nature Reserve). Within each site, the one-ha study plots are outlined. Satellite photographs taken from Google Earth with permission.

Ankasa is located in south-west Ghana, in tropical wet evergreen forest and receives over 2000 mm of rain a year, spread over two rainy seasons—April to July and September to November. Soils are loamy, highly weathered, acidic, and high in aluminium [52]. Data were taken from two 1-ha forest plots; Ankasa 01 located on mature upland soils and Ankasa 03 located in low riverein forest that is periodically inundated during the rainy season. See Table 1 for more details.

Bobiri is located in moist semi-deciduous forest and receives an annual precipitation of approximately 1500 mm, spread over the same two rainy seasons described above. Soils in Bobiri are similarly loamy but less acidic than in Ankasa, and unusually high in base cations. Data were taken from two 1-ha forest plots (Bobiri 01 and Bobiri 02). Bobiri 01 is located within the Strict Nature Reserve with no record of logging. According to Forest Commission (FC) records, Bobiri 02 was last (very lightly) logged in 1959. This comprised of 1–2 stems per hectare, which was rigorously enforced by the FC.

Kogyae is located in the transitional forest zone, with an average rainfall of 1200–1300 mm. To reflect the full extent of the forest–savannah transition landscape, data were taken from three plots—Kogyae 02 located in dry forest, Kogyae 04 located in forest-savannah transition and Kogyae 05 located in woody savanna. Soils in Kogyae are sandy with low water and nutrient retention properties. Similarly to Bobiri, they are high in base cations, either due to local depositional features or Saharan dust deposits, transported during the Harmattan winds [53].

**Table 1.** Meteorological, soil and productivity characteristics for the 3 tropical forest study sites located along a 1200–2000 mm rainfall gradient in Ghana. $P_{total}$ = total soil phosphorus pool. $Ca_{ex}$, $Mg_{ex}$, $K_{ex}$, $Na_{ex}$, $Al_{ex}$ = exchangeable calcium, magnesium, potassium and aluminum concentrations. ±1 standard deviation. Adapted from Moore et al. [52]. See Moore et al. [52] and Gvozdevaite et al. [54] for more details.

| Site Name | Ankasa Conservation Area | Bobiri Forest Reserve | Kogyae Strict Nature Reserve |
|---|---|---|---|
| Latitude (°) | 5.2680 | 6.6910 | 7.3012 |
| Longitude (°) | −2.6955 | −1.3389 | −1.1649 |
| Elevation (m.a.s.l) | 114 | 254 | 225 |
| Mean annual air temperature (°C) | 25 | 25.7 | 26.4 |
| Mean annual precipitation (mm $yr^{-1}$) | 2050 | 1500 | 1200 |
| Mean maximum climatological water deficit (mm) | −13 | −374 | −412 |
| Soil pH | 4.27 | 6.05 | 6.07 |
| Soil N (%) | 0.17 | 0.16 | 0.06 |
| Soil C (%) | 2.61 | 1.71 | 0.72 |
| $P_{total}$ (mg $kg^{-1}$) | 147 | 258 | 67 |
| $Ca_{ex}$ | 1.34 | 32.81 | 18.91 |
| $K_{ex}$ | 0.83 | 1.25 | 1.09 |
| $Mg_{ex}$ | 3.45 | 11.00 | 6.22 |
| $Al_{ex}$ | 18.44 | 0.89 | 0.02 |
| Sand (%) | 63 | 47 | 83 |
| Clay (%) | 22 | 29 | 2 |
| Silt (%) | 15 | 24 | 15 |
| Leaf photosynthesis rate (μmol $m^{-2}$ $s^{-1}$) | 5.87 | 7.75 | 7.74 |
| Leaf residence time (months) | 9–10 | 4–6 | 6.5–8 |
| Aboveground coarse wood residence time (months) | 99 ± 22.1 | 39. 65 ± 8.88 | 40.60 ± 9.08 |
| NPP (Mg C $ha^{-1}$ $yr^{-1}$) | 13.12 ± 0.79 | 11.74 ± 0.95 | 10.19 ± 0.78 |

### 2.2. Leaf Trait Sampling

Fieldwork was carried out between October 2014 and March 2015. In Kogyae, leaf traits were sampled between October and November. In Ankasa and Bobiri, leaf traits were sampled between December and March. Leaf traits were collected as part of the KWAEEMMA traits campaign ('Children of the Forest' in the local Twi language), a collaboration between GEM and the Forestry Research Institute of Ghana. For each one-ha forest plot, the most abundant species were chosen that represented over >55% of the basal area of each plot. From each of these species, the three largest individuals were sampled (based on diameter at breast height [DBH]). From these trees, six leaves were harvested from branches cut down by a professional tree climber; three from a sun branch in the upper canopy located in direct sunlight and three from a branch underneath the main crown located in complete shade. Leaf spectroscopy and trait measurements were collected for all leaves. Across the seven plots, this resulted in leaf spectra and corresponding trait measurements for 753 sun and shade leaves respectively.

Less than 12 h after collection, leaves were scanned using a digital scanner (Canon LiDE 110) to determine their area and then oven dried at 72 °C for three days. LMA was derived by dividing the leaf's dry mass (g) by its fresh one-sided area ($m^2$). The dried leaves were then used for chemical analysis. Leaf chemistry measurements (N, P, K, Ca, Mg) were carried out at Wageningen University using a mass spectrometer (see Moore et al. [52] for more details). All leaf chemical traits are reported on a dry mass basis.

### 2.3. Leaf Spectroscopy Measurements

Hemispheric leaf reflectance measurements were carried out immediately in the field after branch harvesting. Measurements were taken on the adaxial surface of the leaf, halfway between the petiole and leaf tip and at the mid-point between the main vein and leaf edge. Care was taken to avoid large primary or secondary veins. The spectra spanned 750 bands between 325–1075 nm and were collected using an ASD Fieldspec Handheld 2, with fibre optic cable, contact probe and an illumination collimator (Analytical Spectral Devices, Boulder, CO, USA). For each leaf, an average of 25 spectra were taken. Measurements were collected with 136 ms integration time per spectrum. The spectrometer was optimised and calibrated for dark current and white light after every three measurements. The spectra were trimmed at the far edges to remove noise, producing a final range of 400–1050 nm. To control

for outliers, spectra lying more than two standard deviations away from the mean in the visible light (550 nm), or NIR (900 nm), were flagged and checked.

### *2.4. Airborne Spectroscopy*

The airborne imaging data were collected in the first two weeks of March, 2016. Data were taken from both Ankasa plots, and Bobiri 02. No airborne data were taken from Kogyae, as it was late dry season and the trees were mostly leafless.

The airborne imaging data were collected using the WageningenUR HYMSY system—a lightweight hyperspectral mapping system mounted on an octocopter UAV [55]. The HYMSY is comprised of a custom made pushbroom spectrometer (450–950 nm, 9 nm FWHM, 25 lines/s, 328 px/line), a photogrammetric camera, and a miniature GPS Inertial Navigation System. Each plot was covered by between 2–4 flights. The raw hyperspectral data was processed to reflectance factors using the empirical line method [56] with the help of a grey reference panel placed on the forest floor near the UAV take-off position. Using the HYMSY processing chain, each flight produced an RGB orthomosaic at 3 cm resolution, a Digital Surface Model (DSM) at 20 cm resolution, and a hyperspectral datacube at 50 cm resolution. For more details on the processing methodology see Suomalainen et al. [55].

Analysis of the hyperspectral datacube was carried out in Environment for Visualizing Images (ENVI), version 5.3 (Exelis Visual Information Solutions, Boulder, CO, USA). Flight lines over each plot were stitched together using the ENVI mosaicking tool. All pixels with an NDVI < 0.6 were removed to screen out non-vegetation [57]. Shadows were removed by masking out all pixels with a maximum reflectance of less than 0.2 across all wavelengths [58].

Tree crown spectra were manually extracted for each individual tree from which field spectroscopy and trait measurements had been taken, and that exhibited crowns that lay > 50% in direct sunlit (Figure 2). Tree crowns were identified using the RGB orthomosaic, which displayed the forest canopy at high enough resolution to visually distinguish between different trees crowns. The tree crowns recognizable on the RGB orthomosaic were manually matched to the field-sampled trees by using x,y coordinates for each tree, species identification, known crown dimensions, and tree height from the DSM. Overall, this resulted in $n = 58$ for matched tree canopy spectra across all three plots. Tree crowns were manually delineated and identified in accordance with Dalponte et al. [59] who found that the manual identification of tree crowns had a higher accuracy rate than those automatically, or even semi-automatically, delineated and identified from hyperspectral data. Our method was closely aligned with Dalponte et al., Leckie et al. and Clark et al. [59–61], who similarly used tree location, species type, tree height and crown diameter to aerially identify tree crowns.

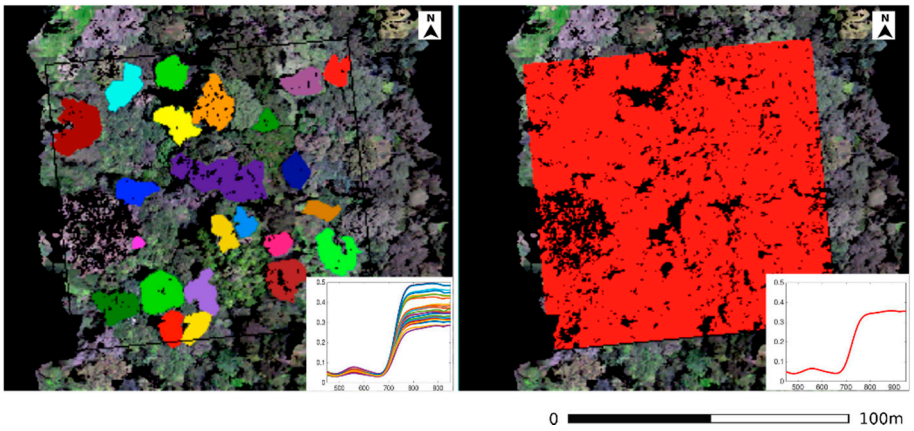


**Figure 2.** (**Left**) Tree crown spectra extracted from Ankasa 01 with NDVI < 0.6 and shadows masked. Spectra were only extracted for trees from which field data were taken and that exhibited crowns that lay > 50% in direct sunlight. (**Right**) Average plot spectrum extracted from Ankasa 01 with NDVI < 0.6 and shadows masked.

An average canopy spectrum for each plot was extracted using geo-referenced plot corner coordinates and the ENVI region of interest tool.

### *2.5. Spectra–Trait Analyses*

To predict leaf traits using the individual sun and shade leaf spectra, we used PLSR analysis. The PLSR method is effective, as it uses the continuous spectrum as a single measurement, rather than carrying out a band-by-band analysis and reduces a large predictor matrix (650 spectral bands between 400–1050 nm) down to a few relatively uncorrelated latent factors [62]. In addition, each part of the spectrum is weighted to determine its relative importance to predicting the foliar trait. We generated predictive models for each trait using the PLSregress function in MATLAB (MathWorks Inc., Natick, MA, USA). To create a completely independent validation dataset, the data was split 70:30 and the PLSR model was calibrated on a randomly selected 70% of the data, with the remaining 30% reserved as an independent testing set. Due to this random component, an average of 30 PLSR runs was taken for each spectra–trait analysis and the results averaged. To avoid overfitting the number of latent factors in each analysis, 30-fold cross validation was used on the calibration dataset. This process iteratively removes one sample from the input data set until the mean square error is minimized. The PLSR models were evaluated using four main metrics—$r^2$ for both the calibration (cal) and independent testing (val) datasets, root mean square error (RMSE), and RMSE as a percentage of the sample mean (%RMSE).

To quantify the airborne spectra–trait relationships, the 58 extracted tree crown spectra were matched with the field-collected sun leaf trait values and run through the same PLSR analysis described above.

### *2.6. Mapping Foliar Traits*

To create maps of predicted canopy traits for each plot, the predictive models generated from the airborne spectra–trait PLSR analyses were applied to each pixel of the hyperspectral plot images using the following formula:

$$Y = b_0 \sum_{i=1}^{101} b_i R(\lambda_i) \quad (1)$$

where $Y$ is the trait value of interest, $b_0$ is the regression coefficient for the intercept computed from the PLSR airborne spectra–trait analyses, the $b_i$ values are the regression coefficients for nanometers 450 through 950 nm at 5 nm intervals, and $R$ is the reflectance value for each band ($\lambda$) of the UAV-collected hyperspectral data [63]. Regression coefficients were taken from the 5 PLSR models that maximized the $r^2$ and minimized the RMSE value, and averaged. As models that maximized the $r^2$ did not always minimize the RMSE (and vice versa), it was found that an average of 5 models performed better than one model alone. A colour palette was added to the results. This generated, to our knowledge, the first maps of tropical forest canopy traits produced using UAV-collected spectra. Maps were only created for 4 out of the 6 leaf traits, as the $r^2$ and RMSE values for K and Mg were considered too weak to carry forward. The maps of predicted canopy LMA, N and P were combined using an RGB composite to generate a map of LES trait interactions.

To investigate the accuracy of the leaf trait maps, the average remotely sensed trait value for each plot was compared with the average field-collected value using $r^2$, RMSE and %RMSE. The field-collected trait values were weighted using a basal-weighted area and stem-weighted abundance method, as well as a simple mean [64]. To evaluate trait relationships, the remotely sensed trait values for all pixels across each plot were analysed using Pearson's correlation.

## 3. Results

### *3.1. Variation in Leaf Traits and Spectral Properties*

Average leaf spectra across Ankasa, Bobiri and Kogyae (Figure 3) demonstrated a very similar shape, magnitude and range, with reflectance peaking in the NIR (700–1075 nm). The spectra showed little difference between sun and shade leaves (Figure 3a,b). Across Ankasa 01, Ankasa 03 and Bobiri 02, the UAV-collected spectra demonstrated a similar shape to the individual leaf level spectra, but with significantly lower reflectance in the visible and NIR regions (Figure 3c–e). The variation in spectra was significantly higher for the UAV-collected spectra (Figure 3f).

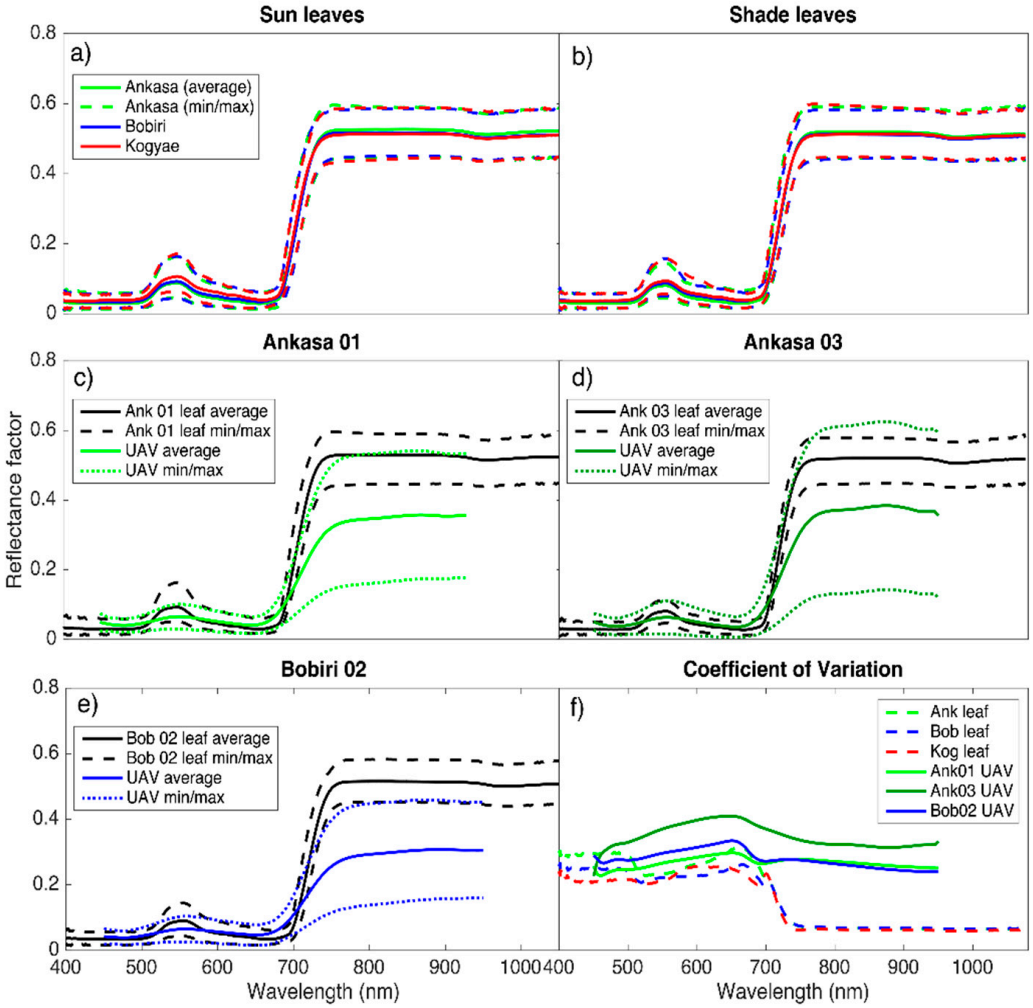


**Figure 3.** (**a**,**b**) Mean, maximum and minimum leaf reflectance spectra of all field-collected sun and shade leaves for Ankasa (green), Bobiri (blue) and Kogyae (red). (**c**–**e**) Mean, maximum and minimum UAV-collected spectra for Ankasa 01 (bright green), Ankasa 03 (dark green) and Bobiri 02 (blue). The corresponding mean, maximum and minimum field-collected sun leaf spectra for the plot is shown in black for comparison purposes. (**f**) Mean coefficient of variation of field-collected sun and shade leaves for Ankasa, Bobiri and Kogyae represented by dashed lines. Mean coefficient of variation of the UAV-collected spectra for Ankasa 01, Ankasa 03 and Bobiri 02 represented by solid lines. The colours follow the same colour key above.

### *3.2. PLSR Analyses*

In the individual sun leaf PLSR analyses, all leaf traits demonstrated a significant ($p < 0.01$) relationship with the leaf reflectance spectra (Table 2). When tested on the independent dataset, LMA

and N demonstrated moderate correlations with the leaf spectra ($r^2$ = 0.42 and 0.43 respectively) and relatively high prediction accuracies of RMSE = 22% and 24%. P and K demonstrated weak but significant correlations with the leaf spectra ($r^2$ = 0.21 and 0.20) and moderate prediction accuracies of RMSE = 34% and 43% respectively. Ca and Mg displayed both weak correlations ($r^2$ = 0.23 and 0.14) and low predictive accuracies (RMSE = 60% and 45%).

Shade leaves displayed much stronger spectra–trait correlations than sun leaves, with all traits showing an increase in $r^2$-val values (Table 2). In some cases these increases were marked, for example LMA $r^2$-val increased from 0.42 to 0.55 and P increased from 0.21 to 0.33. RMSE values decreased slightly for LMA and N and otherwise increased or stayed the same for shade leaves.

The bandwidths most significant for predicting foliar traits differed between sun and shade leaves. For sun leaves, 500–700 nm was the most important region for predicting LMA and N. For shade leaves, the NIR was the most important region for predicting LMA and N, with a strong signal at 700 nm for N (Figure 4. See Figure A1 for shade leaf graphs). Spectral weightings for P mirrored N. Spectral weightings for K, Ca and Mg showed a combination of weightings across the visible, red-edge and NIR regions, indicating that correlations with both LMA and N contributed to their estimates.

When the PLSR analyses were carried out using UAV-collected tree crown spectra, all spectra-trait relationships decreased in strength compared to the individual leaf analyses, with the exception of P and Ca. (Table 2). For LMA, N, K and Mg, the tree crown spectra were able to predict 5–21% less of the variance between average tree crown trait values than at the individual leaf level. Overall, the tree crown spectra were able to predict LMA, N, P and Ca at $p < 0.10$. Using UAV-collected spectra, the weightings showed that the NIR region was the most important part of the spectrum for predicting every trait (Figure 4).

**Table 2.** PLSR results for (i, ii) individual sun and shade leaf spectra. $n$ = 753 for sun and shade leaves respectively. (iii) UAV-collected tree crown spectra. $n$ = 58 for UAV-collected tree crown spectra. RMSE = Root mean square error. $r^2$-cal represents the 70% of data used to create the empirical model and $r^2$-val the 30% of data upon which the model was tested. The level of significance ($p$) is indicated (* $p < 0.10$; ** $p < 0.05$; *** $p < 0.01$). Results are the average of 30 model runs. All field-collected data is reported on a dry mass basis.

| **Leaf Type** | **Sun** | | | | | **Shade** | | | | | **UAV-Collected Spectra** | | | | |
|---|---|---|---|---|---|---|---|---|---|---|---|---|---|---|---|
| **Spectral Range and Resolution** | **Individual Leaves (400–1050 nm) 1 nm FWHM** | | | | | **Individual Leaves (400–1050 nm) 1 nm FWHM** | | | | | **Tree Crowns (450–950 nm) 9 nm FWHM** | | | | |
| | **Mean ± 1 Std** | **RMSE** | **%RMSE** | **$R^2$-cal** | **$R^2$-val** | **Mean ± 1 Std** | **RMSE** | **%RMSE** | **$R^2$-cal** | **$R^2$-val** | **Mean ± 1 Std** | **RMSE** | **%RMSE** | **$R^2$-cal** | **$R^2$-val** |
| LMA (g $m^{-2}$) | 102 ± 35 | 21.13 | 22 | 0.60 *** | 0.42 *** | 89 ± 33 | 19.44 | 20 | 0.70 *** | 0.55 *** | 98 ± 20 | 17.43 | 18 | 0.45 *** | 0.25 * |
| N (%) | 2.05 ± 0.63 | 0.48 | 24 | 0.78 *** | 0.43 *** | 2.07 ± 0.64 | 0.47 | 23 | 0.83 *** | 0.48 *** | 2.15 ± 0.65 | 0.54 | 25 | 0.38 *** | 0.22 * |
| P (%) | 0.12 ± 0.05 | 0.04 | 34 | 0.64 *** | 0.21 *** | 0.12 ± 0.05 | 0.05 | 38 | 0.83 *** | 0.33 *** | 0.10 ± 0.04 | 0.03 | 32 | 0.38 *** | 0.22 * |
| K (%) | 0.89 ± 0.49 | 0.41 | 43 | 0.43 *** | 0.20 *** | 1.03 ± 0.55 | 0.48 | 51 | 0.52 *** | 0.20 *** | 0.91 ± 0.44 | 0.41 | 44 | 0.25 * | 0.15 |
| Ca (%) | 1.39 ± 1.98 | 0.89 | 60 | 0.50 *** | 0.23 *** | 1.57 ± 1.11 | 0.94 | 63 | 0.66 *** | 0.28 *** | 0.87 ± 0.66 | 0.56 | 64 | 0.43 *** | 0.25 * |
| Mg (%) | 0.34 ± 0.17 | 0.16 | 45 | 0.37 *** | 0.14 *** | 0.38 ± 0.19 | 0.18 | 48 | 0.45 *** | 0.16 *** | 0.31 ± 0.18 | 0.18 | 57 | 0.19 | 0.09 |

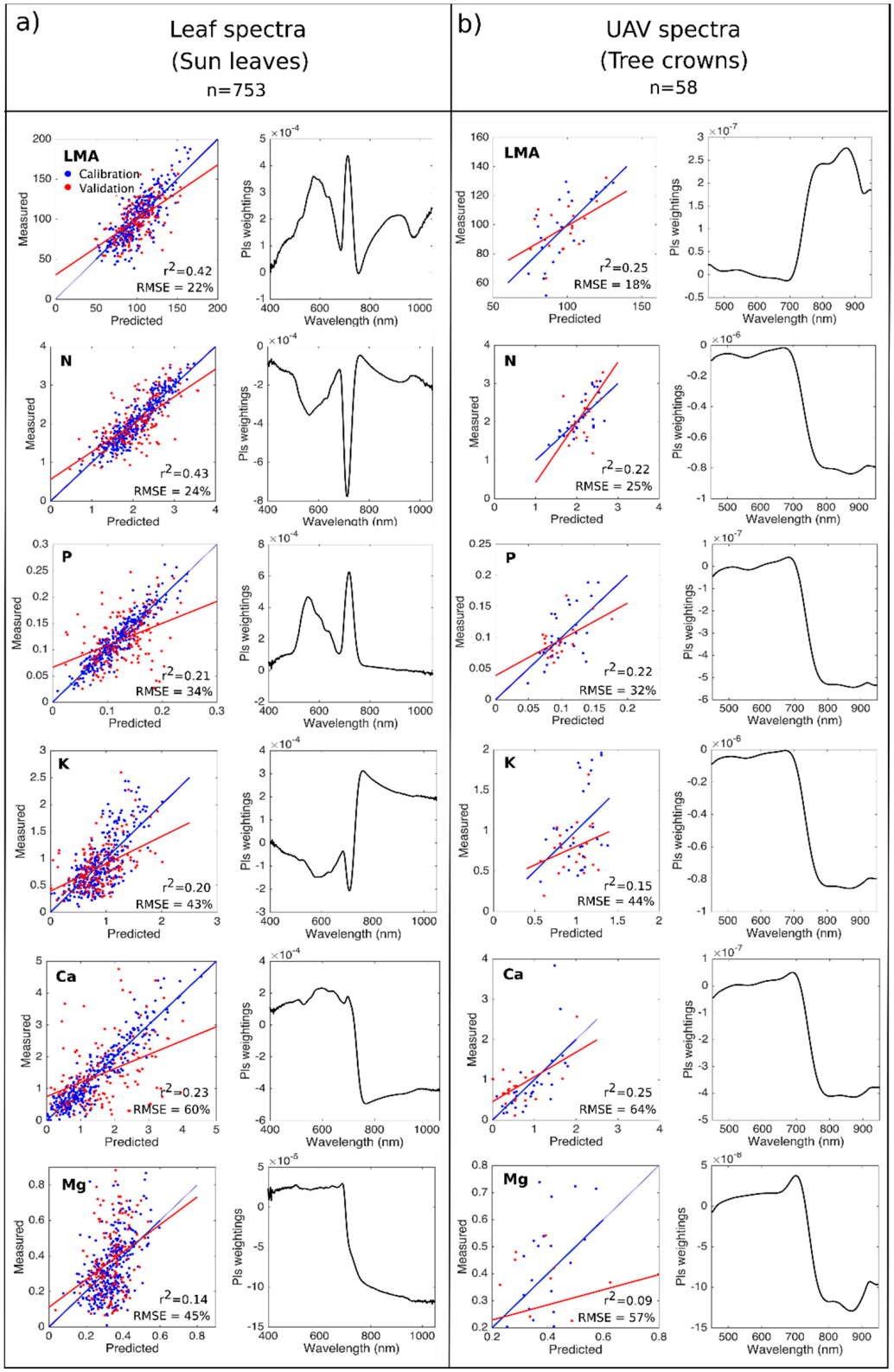


**Figure 4.** (**a**, **left**) Relationships between measured and predicted leaf traits using individual sun leaf reflectance spectra and PLS regression analysis. $n$ = 753. Blue line = $r^2$-cal regression line. Red line = $r^2$-val regression line. RMSE and $r^2$-val values displayed on graph. (**a**, **right**) PLSR spectral weightings for each leaf trait. Deviation from 0 indicates the parts of the spectrum that most strongly influence the empirical model. (**b**) The same as (**a**), but using UAV-collected reflectance spectra of 58 tree crowns.

### *3.3. Mapping Foliar Traits Using UAV-Collected Hyperspectral Data*

The maps of predicted leaf traits (Figure 5) display similar trait values for Ankasa 01 and Ankasa 03. In Bobiri 02, the maps display much higher N, P and Ca values than in Ankasa. All results were supported by the field-collected values (Table 3), the one exception being lower LMA in Ankasa 01, which was not found in the weighted field samples.

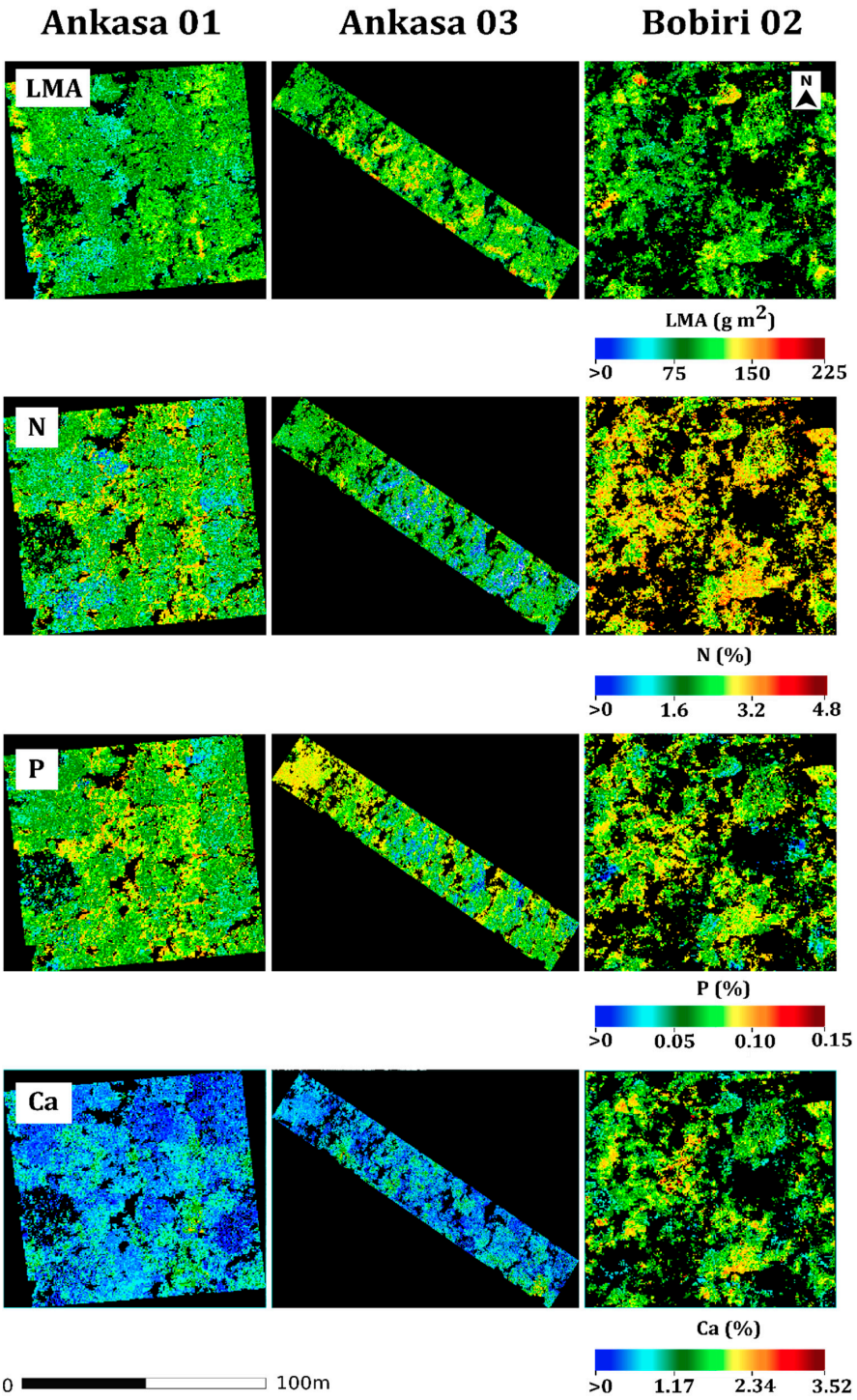


**Figure 5.** Maps of forest canopy LMA, N, P and Ca for three one-ha tropical forest plots in Ghana, West Africa. Created using the regression coefficients generated from the PLSR analyses in Table 2, applied to each pixel of the hyperspectral canopy data using Formula (1). Black areas represent shadows or areas with an NDVI < 0.6. Pixel resolution = 0.5 m.

**Table 3.** Average predicted foliar traits (bold) for three one-ha tropical forest plots. Calculated using UAV-collected hyperspectral data and PLSR analysis. Field-collected trait values are shown for comparison purposes. The field-collected data have been weighted using three methods: basal-area-weighting, stem-abundance-weighting and no weighting. The root mean square error (RMSE), percentage root mean square error (%RMSE) and $r^2$ values of predicted vs. field-collected traits are shown for each method of weighting. ($n$ = 3). The level of significance ($p$) is indicated (* $p < 0.10$; ** $p < 0.05$; *** $p < 0.01$). Significant differences ($p < 0.01$) between the predicted trait values of each plot are denoted using the letters $^{a–c}$ Where necessary, values have been rounded to two decimal places.

| **Predicted Trait (Bold) vs. Field-Collected Value** | **Plot** | | | **Statistics** | | |
|---|---|---|---|---|---|---|
| | **Ankasa 01** | **Ankasa 03** | **Bobiri 02** | **RMSE** | **%RMSE** | **$R^2$** |
| Field-sampled basal area (%) | 63 | 56 | 61 | | | |
| LMA (g $m^{-2}$) | 90 ± 19 $^a$ | 100 ± 24 $^b$ | 98 ± 20 $^c$ | - | - | - |
| Basal-area-weighted | 102 | 101 | 94 | 7 | 8 | 0.19 |
| Stem-abundance-weighted | 101 | 101 | 92 | 7 | 8 | 0.11 |
| Unweighted | 97 | 101 | 100 | 6 | 5 | 1 *** |
| N (%) | 1.97 ± 0.64 $^a$ | 1.74 ± 0.76 $^b$ | 2.93 ± 0.50 $^c$ | - | - | - |
| Basal-area-weighted | 2.06 | 1.93 | 2.74 | 0.16 | 7 | 1 *** |
| Stem-abundance-weighted | 2.00 | 1.89 | 2.81 | 0.11 | 11 | 1 *** |
| Unweighted | 1.91 | 2.03 | 2.45 | 0.33 | 15 | 0.85 |
| P (%) | 0.07 ± 0.02 $^a$ | 0.07 ± 0.02 $^b$ | 0.08 ± 0.02 $^c$ | - | - | - |
| Basal-area-weighted | 0.09 | 0.10 | 0.15 | 0.05 | 74 | 0.98 |
| Stem-abundance-weighted | 0.09 | 0.10 | 0.15 | 0.05 | 74 | 0.98 |
| Unweighted | 0.08 | 0.10 | 0.13 | 0.04 | 62 | 0.84 |
| Ca (%) | 1.20 ± 0.36 $^a$ | 1.34 ± 0.48 $^b$ | 1.87 ± 0.50 $^c$ | - | - | - |
| Basal-area-weighted | 0.72 | 0.74 | 1.82 | 0.45 | 30 | 0.97 |
| Stem-abundance-weighted | 0.73 | 0.73 | 1.88 | 0.45 | 30 | 0.96 |
| Unweighted | 0.71 | 0.86 | 1.54 | 0.44 | 44 | 1 *** |

Similarly to Asner et al. [64], this study finds that, in general, the method for weighting the field data (basal-area-weighted, stem-abundance-weighted or unweighted mean) had very little effect on the strength, magnitude or direction of the relationships with the UAV data (Table 3). One exception was LMA, where an unweighted mean resulted in an $r^2$ value of 1, compared to 0.19 and 0.11 for the basal-area-weighted and stem-abundance-weighted mean respectively. Aside from LMA, however, all field-based trait values showed positive relationships with the remotely sensed plot predictions, with $r^2$ values ranging from 0.84–1.

### *3.4. Leaf Economic Spectrum Trait Interactions*

The RGB composite of predicted LMA, N and P showed that the majority of trees in Ankasa 01 and Ankasa 03 fall on the 'slow growing but enduring' end of the LES (Figure 6). The general hue of both plots is dark blue to purple, representing high LMA, low N and varying P. In contrast, the majority of trees in Bobiri fall on the 'live fast die young' end of the LES, with the plot displaying a general yellow hue, representing low LMA, high N and high P. Within this generality, however, there are still some diverse trait strategies, with prominent tree crowns in Ankasa displaying low LMA, low N and high P, and clusters of foliage in Bobiri displaying high LMA, high N and low P.

At the individual pixel level, no plot displayed a significant relationship between LMA and N values (Figure 7). All plots displayed a significantly positive correlation ($p < 0.01$) between N and P values ($r^2$ = 0.63, 0.59, 0.44), and a significantly negative correlation between LMA and P values, with Bobiri 02 displaying a comparatively strong relationship of $r^2$ = 0.26. All plots displayed significantly positive correlations between LMA and Ca, and inverse relationships between N and Ca, and P and Ca.

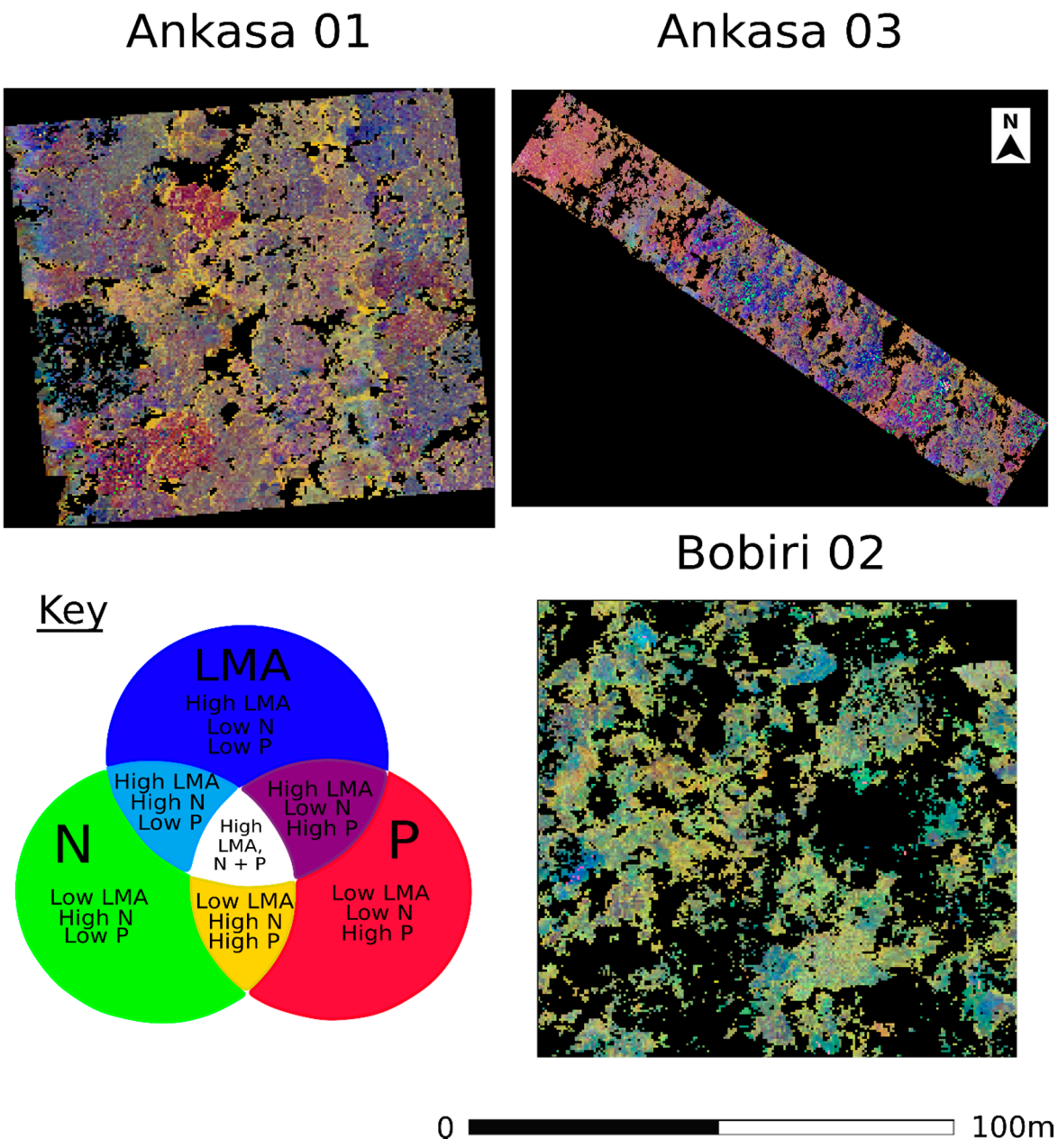


**Figure 6.** RGB composite of LES trait interactions (red = P, green = N, blue = LMA). Produced using the maps of predicted canopy LMA, N and P in Figure 4. Black areas represent shadows or areas with an NDVI < 0.6. In the Venn diagram, the continuous rgb colour scheme is shown as discrete categories for ease of interpretation. Pixel resolution = 0.5 m.

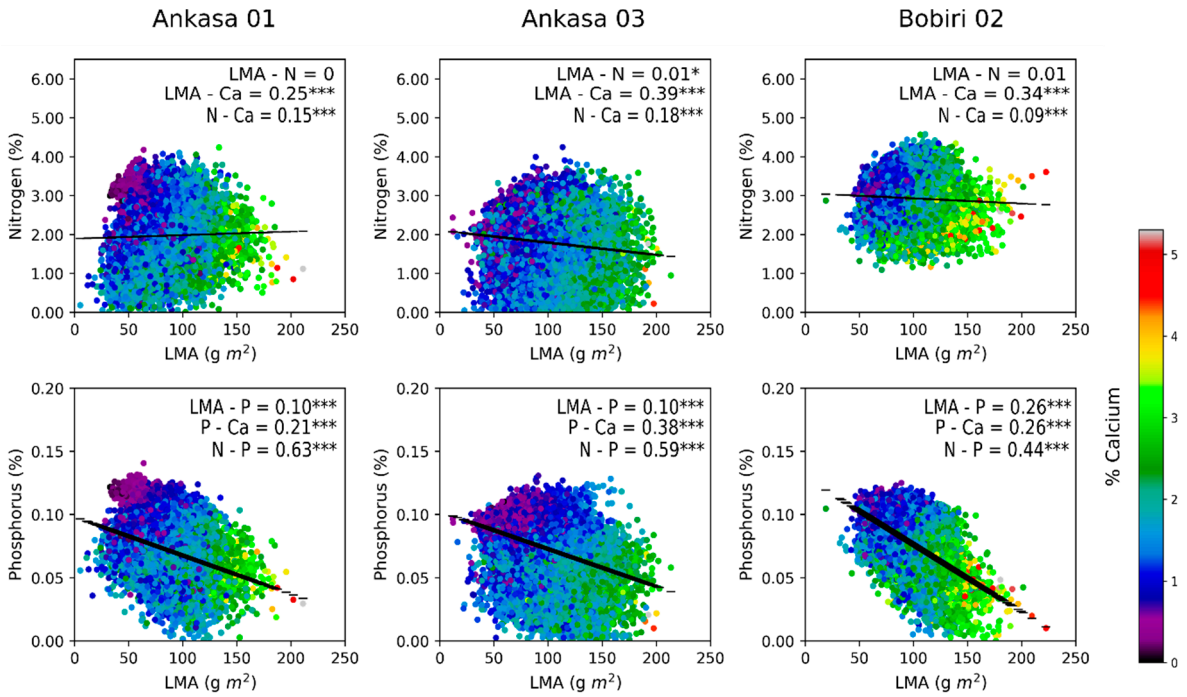


**Figure 7.** Relationship between LMA–N and LMA–P for each pixel of Figure 6. Colour as a function of Ca. $R^2$ values are shown on the graphs with the level of significance ($p$) indicated (* $p < 0.10$; ** $p < 0.05$; *** $p < 0.01$). $n$ = 34789 for Ankasa 01. $n$ = 32807 for Ankasa 03. $n$ = 19014 for Bobiri 02. These graphs are based on the remotely sensed values, not field-collected data.

## 4. Discussion

This study demonstrates the potential of using leaf spectral properties and UAVs to scale up from individual leaves to landscapes. Calibrated on a field campaign that measured the trait values of 753 sun leaves, we used UAV-collected VNIR hyperspectral data to map LMA, N, P and Ca across three hectares of diverse tropical forest, revealing patterns of trait variation both between and within forest sites. While this study limited itself to analysing interactions between LES traits and validating the methodology, it demonstrates the potential of UAV-collected spectra for scaling up similar leaf trait-based work. For example, LMA and leaf chemical traits have been shown to be good indicators of canopy phylogeny [65,66], invasive species [50], decomposition rates [67,68], soil fertility [69] and drought tolerance [15].

When compared to the individual leaf spectra, the UAV-collected spectra displayed a similar shape, but lower reflectance in the visible and NIR regions (Figure 3). This is to be expected. Increased leaf area index and variable leaf angle distribution in the canopy causes multiple scattering and the increased absorption of light compared to single leaves. The UAV-collected spectra also displayed significantly higher variation than the hand-collected spectra. This is almost certainly due to the far higher number of spectra pixels recorded across each plot—34,789 pixels across Ankasa 01, compared to 352 hand-collected leaf spectra. While only healthy, mature sun and shade leaves were measured by hand, the UAV captured all visible sun foliage across the plot, including leaves of different ages, health and species. Leaf age has been shown to have a significant effect on spectral properties [70], as has leaf health [71,72]. The individual sun and shade leaf spectra were collected from 60 species representing 27 families across the three plots. While these species represented >55% of the basal area of each plot, there were a total of 130 species from 51 families present across the three plots, contributing to far higher spectral variation in the UAV spectral data.

Significant relationships were found between LMA, N, P, K, Ca, Mg and leaf reflectance spectra at the individual leaf level (Table 2). These were strongest for the directly estimated traits of LMA and N. The covariate relationships found between LMA, N and the indirectly expressed nutrients

are discussed in more detail below. Results were slightly lower than those found by Asner et al. [37], who used a very similar spectral range and method, but a much larger and more diverse sample size, suggesting that high ecological variety drives stronger PLSR relationships.

Across all traits, shade leaves demonstrated much stronger spectral relationships than sun leaves (Table 2). In the spectroscopy literature, shade leaves are chronically understudied. Among the few studies that include shade leaves in their analysis however, this finding does not appear to be unique. Using PLSR to predict leaf age in a Peruvian and Brazilian forest, Wu et al. [73] found that on a species-by-species basis, shade leaves predicted 5–27% more of the variance in LMA than sun leaves and 6–28% more of the variance in leaf water content.

The higher performance of shade leaves may be linked to their structure. To increase light capture efficiency, shade leaves are thinner, possess fewer cells per leaf area than sun leaves and have palisade cells of roughly equal dimensions that concentrate chloroplasts in a dense layer on the leaf's adaxial surface. In contrast, sun leaves are thicker, with multiple mesophyll layers and columnar palisade cells to allow light to pass through vacuoles and the spaces between cells and reach chloroplasts in the spongy mesophyll [74,75]. Thus, a beam of light penetrating a sun leaf has more cell–wall–air interfaces to pass through and a longer path length, increasing the probability of being scattered and absorbed, and potentially decreasing the signal-to-noise ratio of the reflectance spectra. The fact that shade leaf–trait relationships are equal or stronger than sun leaf–trait relationships is important, because shade leaves constitute the majority of tropical foliage and influence canopy spectral signatures in the NIR—hence, their spectral contribution will assume greater importance when the spectral range of the UAV-collected data is extended up to 2500 nm.

Scaling up to the airborne level, LMA, N, P and Ca demonstrated a significant (at $p < 0.10$) relationship with the UAV-collected tree crown spectra (Table 2). These relationships were generally lower than those at found at the individual leaf level. This may be due to several reasons. Firstly, the PLSR analyses were carried out with a much smaller sample size of tree crowns—58 tree crowns vs. 753 individual leaves. Although PLSR analyses have been carried out with similar sample sizes (e.g., [33]), results have been shown to improve with increasing sample size, until stabilization is reached at $n = 1000$ [37]. Secondly, the airborne canopy data were collected 52–64 weeks after the field collection campaign. Interannual variability of leaf traits has been found to be low for LMA and leaf nutrient values collected at the same time of year or in the same season [76–78]. Yet, when the airborne canopy data were collected, tree crown trait values may still have altered slightly from their field-collected values. As the PLSR method works by calibrating and predicting values based on spectral variability, slight inaccuracies in crown trait values would weaken the PLSR results. It is important to note that we do not list these factors to undermine the study, but rather to give further confidence in its results. The fact that, notwithstanding these limitations, we found significant spectra–tree crown relationships for 4 out of 6 traits, supporting the value of using UAVs to estimate canopy traits.

In addition to the factors above, we hypothesize that the largest improvements in airborne spectra–trait relationships will be made when the SWIR (700–2500 nm) region is included in the canopy spectra measurements. Using the full VSWIR range has been shown to significantly increase spectra–trait relationships [37,79–81], as the majority of traits have significant expressions in the short-wave infrared spectrum. Airborne hyperspectral sensors covering the full 400–2500 nm range are commercially available [82]. Alternatively, combining information from multiple hyperspectral sensors is possible [83], and would also provide all the relevant bands. Experimenting with the expanding field of nonlinear transformation methods (often referred to as machine learning algorithms) may also improve retrieval rates [84], although in this study PLSR was used as it offers a more transparent, physical approach to quantifying spectra-trait relationships and facilitates comparisons with similar studies.

At the whole plot level, the UAV-predicted plot averages showed good agreement with field-collected values (Table 3). With the exception of LMA, basal area- and stem-abundance weighting

of field-collected traits generally demonstrated similar or higher $r^2$ values, and similar or lower %RMSE values, than the unweighted means. This supports the use of weighting field data when calibrating or validating remotely sensed variables. Despite the fact that few regression models were statistically significant, this is more likely due to the extremely small sample size (3 data points) than to a lack of agreement between the field-collected and remotely sensed values. Weighted LMA was the only field-collected trait not to demonstrate a positive relationship with the remotely sensed canopy values. However, unlike N, P or Ca, variations in LMA were small between the three sites. The remotely sensed values demonstrated an uncertainty of 19–24 g $m^2$—larger than the variation observed between the three sites. Thus, it is unsurprising that the field and remote sensing approaches do not agree on a mean LMA trend for these 3 plots—greater LMA variation is required.

The fact that the UAV-collected data were able to quantify average trait values for each plot represents an important step in scaling up these results. One-ha tropical forest study plots are not always representative of their host landscapes [64,85]. Thus, while UAVs could be calibrated on field results collected from smaller study sites, their greatest asset in is mapping these values over larger areas, where field-collection is impractical.

Across the three sites, the observed three-way interaction between LMA, N and P supports the proposal of a multi-trait LES, sensitive to climatic and edaphic constraints [48,86,87]. From the RGB composite, it can be seen that Ankasa 01 and Ankasa 03 generally display high LMA, low N and low P values, while Bobiri 02 generally exhibits low LMA, high N and high P values. This is almost certainly due to the strong rainfall gradient found across West Africa. While increasing precipitation is generally associated with more favourable conditions and trait trade-offs that favour fast growth and short mortality, at high precipitation rates (over 2000 mm), nutrient gradients have been found to interact with precipitation gradients. High precipitation causes soil nutrient leaching, promoting the selection of species for traits on the persistent end of the economics spectrum [88–90]. Evergreenness has been found to be a response to the relatively low nutrient availability in very wet tropical forest, as increased leaf longevity is an effective nutrient conservation mechanism, resulting in a longer photosynthetic season and a reduced demand on the amount of soil nutrients required to replace leaves [91–93]. Hence, with their weathered tropical soils promoting the growth of evergreen species, Ankasa 01 and Ankasa 03 demonstrate high LMA values, high leaf longevity (9–12 months) and lower N, P and Ca values. These leaf strategies are not limited to plant foliage, but are mirrored by the tree's overall performance. According to the carbon cycling data for the plots, Ankasa demonstrates high wood residence rates (99 $\pm$ 22.1 years in Ankasa 01) and lower NPP (13.3 $\pm$ 0.6 Mg C $ha^{-1}$ $year^{-1}$: all data from Moore et al. [52]. See Table 1).

In contrast, the RGB composite shows that the most common trait strategy in Bobiri represents the 'live fast die young' end of the LES spectrum. Here, lower mean annual rainfall reduces soil leaching rates, while still providing enough water for fast growth. Photosynthetic rates in Bobiri 02 are correspondingly higher, with an average $A_{sat}$ rate of 7.92 µmol $m^{-2}$ $s^{-1}$, compared to an average of 5.65 for Ankasa 01 [54]. Richer soils support a higher number of deciduous tree species—if the resources to build new organic matter are there, there are no constraints to adopting higher rates of leaf production throughout the year. Thus, leaf longevity in Bobiri is lower than in Ankasa (5–6 months), along with wood residence rates (32 $\pm$ 7.16 years), while NPP is higher (16.7 $\pm$ 0.6 Mg C $ha^{-1}$ $year^{-1}$: all data from Moore et al. [52]. See Table 1).

In contrast to the majority of leaf trait studies, our findings were unique in that we did not find a significant relationship between LMA and N across any of the three plots. Here, these relationships are based on the remotely sensed data, yet the same has been found in the field-data [54]. This is probably due to the small spatial distribution of our data. While most studies analysing LMA–N interactions collect data over environmental gradients [94–97], our study focused on trait interactions within fairly homogenous one-ha plots. Thus, while LMA and N values may respond to similar environmental variables over wider areas, under more constant environmental conditions, they appear to be ordered by different controls and do not correlate at the individual leaf level.

Significant relationships were found between all other traits. Bobiri 02 displayed a comparatively strong relationship between LMA and P ($r^2$ = 0.26), supporting research that finds, when soil P is high, phylogeny exerts a stronger control on foliar P than when soil P is limited [66,87]. As both Ankasa sites also display relatively high soil P values compared to many Amazonian soils, a phylogentic ordering of P along the same lines as a phylogenetic ordering of LMA may explain why significant relationships were also found between LMA and P at these sites. As widely reported in the LES literature, N and P exhibited strongly positive relationships in each plot, lending weight to the idea of a stoichiometric link between N and P [86,95,98]. LMA and Ca also demonstrated significantly positive relationships in each plot, probably due to the role of Ca in foliar cell wall development [99]—as LMA increases, more Ca is required.

Overall, our results support the use of a multi-trait LES incorporating P and Ca values [11,51]. In accordance with Asner et al. [48], we find that environmental filters generate more diverse plant trait strategies than be captured by a universal leaf LMA–N relationship and caution against using simple N–LMA tradeoffs to analyse ecosystem function.

## 5. Conclusions

In this study, we show that LMA and multiple leaf chemical traits can be retrieved from individual leaf and plot level spectra using hand-held instruments and UAVs. Retrieval of foliar traits at the tree crown level was weaker. The next steps are to mount both a VNIR and SWIR sensor onto a UAV to increase trait estimation accuracy and attempt to expand the range of quantifiable traits. The next generation of hyperspectral satellites—EnMAP, FLEX, HISUI, HyspIRI, PRISMA, SHALOM [100–105]—will be critical in providing global coverage and monitoring of functional diversity. In the meantime, developing cheaper and easier ways to map leaf traits in tropical forests will provide invaluable data for understanding LES traits and their interactions, as well as helping to inform the next generation of dynamic vegetation and climate models [18,106].

**Author Contributions:** Conceptualization, E.R.T., Y.M. and C.E.D.; Formal analysis, E.R.T.; Funding acquisition, Y.M. and C.E.D.; Investigation, H.B., I.O., A.G., T.P., J.S. (Juha Suomalainen), J.Q., J.S. (John Seidu), C.A., A.J.A., M.H. and S.A.-B.; Project administration, Y.M., M.H., S.A.-B. and C.E.D.; Supervision, Y.M. and C.E.D.; Writing-original draft, E.R.T.; Writing-review & editing, Y.M., H.B., I.O., A.G., J.S. (Juha Suomalainen), A.J.A., M.H., S.A.-B. and C.E.D.

**Funding:** This research was funded by a Google Earth Engine Research Award to C.E.D., E.R.T. and A.J.A. (PRQ22909209), and a NERC DTP student grant to E.R.T. (NE/L002612/1). The UAV data collection was funded by INTERREG V A-project SPECTORS (Project number: 143081). The HYMSY development was funded by INTERREG project 'Smart Inspectors' (Project number: I-1-03 = 176). The field-collected trait data was funded by the Royal Society–Leverhulme Africa Capacity Building Award (AA130026), and an Advanced Investigator Award to Y.M. from the European Research Council (GEM-TRAIT; Grant No. 321131). Y.M. is supported by the Jackson Foundation. The APC was funded by an Oxford RCUK Open Access Block Grant.

**Acknowledgments:** This work is a product of the Global Ecosystems Monitoring (GEM) network (gem.tropicalforests.ox.ac.uk). The UAV data was collected by Wageningen UR Unmanned Aerial Remote Sensing Facility (http://www.wageningenur.nl/uarsf). We thank the FORIG and Ankasa National Park for providing logistical support.

**Conflicts of Interest:** The authors declare no conflict of interest. The funding sponsors had no role in the design of the study; in the collection, analyses, or interpretation of data; in the writing of the manuscript, and in the decision to publish the results.

## Appendix A

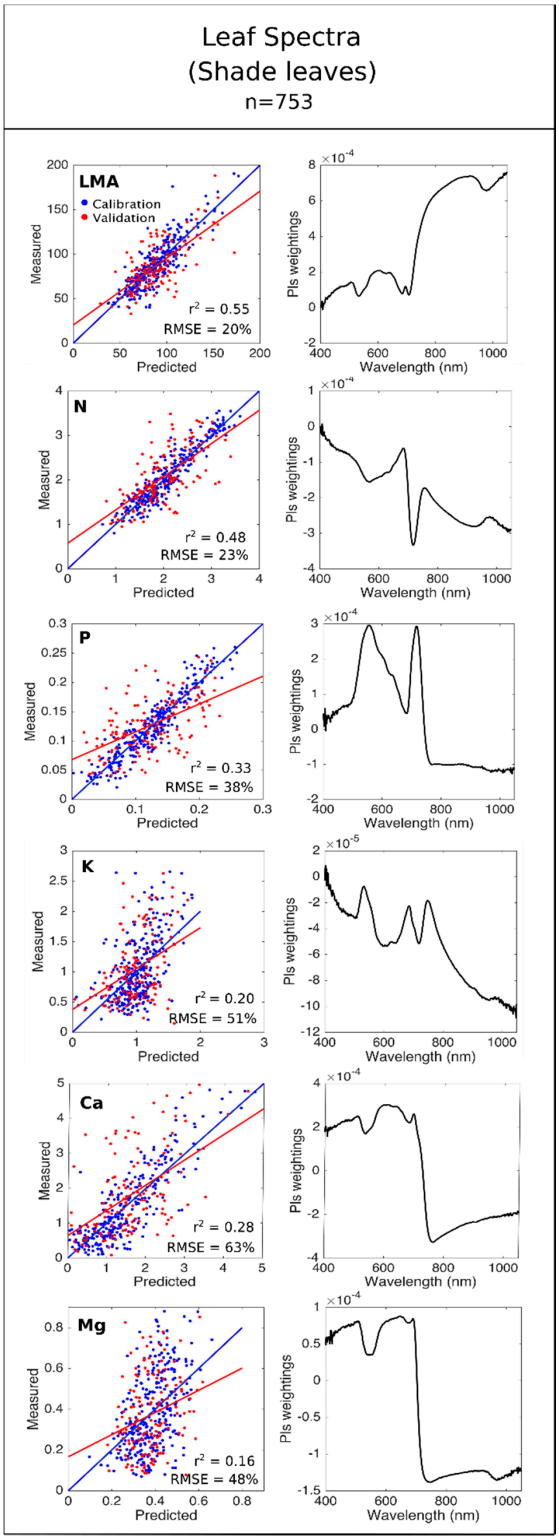


**Figure A1.** (**left**) Relationships between measured and predicted leaf traits using shade leaf reflectance spectra from Figure 2 and PLS regression analysis. $n$ = 753. Blue line = $r^2$-cal regression line. Red line = $r^2$-val regression line. RMSE and $r^2$-cal values displayed on graph. (**right**) PLSR spectral weightings for each leaf trait. Deviation from 0 indicates the parts of the spectrum that most strongly influence the empirical model.

## References


1. Kattge, J.; Diaz, S.; Lavorel, S.; Prentice, I.C.; Leadley, P.; Bönisch, G.; Garnier, E.; Westoby, M.; Reich, P.B.; Wright, I.J.; et al. TRY—A global database of plant traits. *Glob. Chang. Biol.* **2011**, *17*, 2905–2935. [CrossRef]
2. Diaz, S.; Hodgson, J.; Thompson, K.; Cabido, M.; Cornelissen, J.H.C.; Jalili, A.; Montserrat-Marti, G.; Grime, J.P.; Zarrinkamar, F.; Asri, Y.; et al. The plant traits that drive ecosystems: Evidence from three continents. *J. Veg. Sci.* **2004**, *15*, 295–304. [CrossRef]
3. McGill, B.J.; Enquist, B.J.; Weiher, E.; Westoby, M. Rebuilding community ecology from functional traits. *Trends Ecol. Evol.* **2006**, *21*, 178–185. [CrossRef] [PubMed]
4. Lavorel, S.; Grigulis, K.; Lamarque, P.; Colace, M.; Garden, D.; Girel, J.; Pellet, G.; Douzet, R. Using plant functional traits to understand the landscape distribution of multiple ecosystem services. *J. Ecol.* **2011**, *99*, 135–147. [CrossRef]
5. Enquist, B.J.; Norberg, J.; Bonser, S.P.; Violle, C.; Webb, C.T.; Henderson, A.; Sloat, L.L.; Savage, V.M. Chapter Nine—Scaling from traits to ecosystems: Developing a general trait driver theory via integrating trait-based and metabolic scaling theories. In *Advances in Ecological Research*; Pawar, G.W.S., Anthony, I.D., Eds.; Academic Press: San Diego, CA, USA, 2015; pp. 249–318.
6. Díaz, S.; Kattge, J.; Cornelissen, J.H.C.; Wright, I.J.; Lavorel, S.; Dray, S.; Reu, B.; Kleyer, M.; Wirth, C.; Prentice, I.C.; et al. The global spectrum of plant form and function. *Nature* **2016**, *529*, 167–171. [CrossRef] [PubMed]
7. Webb, C.T.; Hoeting, J.A.; Ames, G.M.; Pyne, M.I.; LeRoy Poff, N. A structured and dynamic framework to advance traits-based theory and prediction in ecology. *Ecol. Lett.* **2010**, *13*, 267–283. [CrossRef] [PubMed]
8. Drenovsky, R.E.; Grewell, B.J.; D'antonio, C.M.; Funk, J.L.; James, J.J.; Molinari, N.; Parker, I.M.; Richards, C.L. A functional trait perspective on plant invasion. *Ann. Bot.* **2012**, *110*, 141–153. [CrossRef] [PubMed]
9. Lavorel, S.; Storkey, J.; Bardgett, R.D.; Bello, F.; Berg, M.P.; Roux, X.; Moretti, M.; Mulder, C.; Pakeman, R.J.; Díaz, S.; et al. A novel framework for linking functional diversity of plants with other trophic levels for the quantification of ecosystem services. *J. Veg. Sci.* **2013**, *24*, 942–948. [CrossRef]
10. Reich, P.B.; Walters, M.B.; Ellsworth, D.S. From tropics to tundra: Global convergence in plant functioning. *Proc. Natl. Acad. Sci. USA* **1997**, *94*, 13730–13734. [CrossRef] [PubMed]
11. Wright, I.J.; Reich, P.B.; Westoby, M.; Ackerly, D.D.; Baruch, Z.; Bongers, F.; Cavender-Bares, J.; Chapin, T.; Cornelissen, J.H.; Diemer, M.; et al. The worldwide leaf economics spectrum. *Nature* **2004**, *428*, 821–827. [CrossRef] [PubMed]
12. Santiago, L.S. Extending the leaf economics spectrum to decomposition: Evidence from a tropical forest. *Ecology* **2007**, *88*, 1126–1131. [CrossRef] [PubMed]
13. Cornwell, W.K.; Cornelissen, J.H.; Amatangelo, K.; Dorrepaal, E.; Eviner, V.T.; Godoy, O.; Hobbie, S.E.; Hoorens, B.; Kurokawa, H.; Pérez-Harguindeguy, N.; et al. Plant species traits are the predominant control on litter decomposition rates within biomes worldwide. *Ecol. Lett.* **2008**, *11*, 1065–1071. [CrossRef] [PubMed]
14. Hoffmann, W.; Franco, A.; Moreira, M.; Haridasan, M. Specific leaf area explains differences in leaf traits between congeneric savanna and forest trees. *Funct. Ecol.* **2005**, *19*, 932–940. [CrossRef]
15. Poorter, L.; Markesteijn, L. Seedling traits determine drought tolerance of tropical tree species. *Biotropica* **2008**, *40*, 321–331. [CrossRef]
16. Poorter, L.; Bongers, F. Leaf traits are good predictors of plant performance across 53 rain forest species. *Ecology* **2006**, *87*, 1733–1743. [CrossRef]
17. Sterck, F.J.; Poorter, L.; Schieving, F. Leaf traits determine the growth-survival trade-off across rain forest tree species. *Am. Nat.* **2006**, *167*, 758–765. [CrossRef] [PubMed]
18. Sakschewski, B.; Bloh, W.; Boit, A.; Rammig, A.; Kattge, J.; Poorter, L.; Peñuelas, J.; Thonicke, K. Leaf and stem economics spectra drive diversity of functional plant traits in a dynamic global vegetation model. *Glob. Chang. Biol.* **2015**, *21*, 2711–2725. [CrossRef] [PubMed]
19. Jetz, W.; Cavender-Bares, J.; Pavlick, R.; Schimel, D.; Davis, F.W.; Asner, G.P.; Guralnick, R.; Kattge, J.; Latimer, A.M.; Moorcroft, P.; et al. Monitoring plant functional diversity from space. *Nat. Plants* **2016**, *2*, 1–5. [CrossRef]
20. Asner, G.P.; Martin, R.E.; Anderson, C.B.; Knapp, D.E. Quantifying forest canopy traits: Imaging spectroscopy versus field survey. *Remote Sens. Environ.* **2015**, *158*, 15–27. [CrossRef]

21. Dixon, R.K.; Brown, S.; Houghton, R.E.A.; Solomon, A.; Trexler, M.; Wisniewski, J. Carbon pools and flux of global forest ecosystems. *Science* **1994**, *263*, 185–189. [CrossRef] [PubMed]
22. Pan, Y.; Birdsey, R.A.; Fang, J.; Houghton, R.; Kauppi, P.E.; Kurz, W.A.; Phillips, O.L.; Shvidenko, A.; Lewis, S.L.; Canadell, J.G.; et al. A large and persistent carbon sink in the world's forests. *Science* **2011**, *333*, 988–993. [CrossRef] [PubMed]
23. Ciais, P.; Sabine, C.; Bala, G. Carbon and other biogeochemical cycles. In *Climate Change 2013: The Physical Science Basis. Contribution of Working Group I to the Fifth Assessment Report of the Intergovernmental Panel on Climate Change*; Stocker, T.F., Qin, D., Plattner, G.-K., Eds.; Cambridge University Press: Cambridge, NY, USA, 2013; pp. 465–544. [CrossRef]
24. Jobbágy, E.G.; Jackson, R.B. The vertical distribution of soil organic carbon and its relation to climate and vegetation. *Ecol. Appl.* **2000**, *10*, 423–436. [CrossRef]
25. Lewis, S.L.; Lopez-Gonzalez, G.; Sonké, B.; Affum-Baffoe, K.; Baker, T.R.; Ojo, L.O.; Phillips, O.L.; Reitsma, J.M.; White, L.; Comiskey, J.A.; et al. Increasing carbon storage in intact African tropical forests. *Nature* **2009**, *457*, 1003–1006. [CrossRef] [PubMed]
26. Gates, D.M.; Keegan, H.J.; Schleter, J.C.; Weidner, V.R. Spectral properties of plants. *Appl. Opt.* **1965**, *4*, 11–20. [CrossRef]
27. Knipling, E.B. Physical and physiological basis for the reflectance of visible and near near-infrared radiation from vegetation. *Remote Sens. Environ.* **1970**, *1*, 155–159. [CrossRef]
28. Curran, P.J. Remote sensing of foliar chemistry. *Remote Sens. Environ.* **1989**, *30*, 271–278. [CrossRef]
29. Kokaly, R.F. Investigating a physical basis for spectroscopic estimates of leaf nitrogen concentration. *Remote Sens. Environ.* **2001**, *75*, 153–161. [CrossRef]
30. Smith, M.; Martin, M.E.; Plourde, L.; Ollinger, S.V. Analysis of hyperspectral data for estimation of temperate forest canopy nitrogen concentration: Comparison between an airborne (AVIRIS) and a spaceborne (hyperion) sensor. *IEEE Trans. Geosci. Remote Sens.* **2003**, *41*, 1332–1337. [CrossRef]
31. Asner, G.P.; Martin, R.E.; Ford, A.J.; Metcalfe, D.J.; Liddell, M.J. Leaf chemical and spectral diversity in Australian tropical forests. *Ecol. Appl.* **2009**, *19*, 236–253. [CrossRef] [PubMed]
32. Asner, G.P.; Martin, R.E.; Tupayachi, R.; Emerson, R.; Martinez, P.; Sinca, F.; Powell, G.V.N.; Wright, S.J.; Lugo, A.E. Taxonomy and remote sensing of leaf mass per area (LMA) in humid tropical forests. *Ecol. Appl* **2011**, *21*, 85–98. [CrossRef] [PubMed]
33. Doughty, C.E.; Asner, G.P.; Martin, R.E. Predicting tropical plant physiology from leaf and canopy spectroscopy. *Oecologia* **2011**, *165*, 289–299. [CrossRef] [PubMed]
34. Asner, G.P.; Martin, R.E. Spectranomics: Emerging science and conservation opportunities at the interface of biodiversity and remote sensing. *Glob. Ecol. Conserv.* **2016**, *8*, 212–219. [CrossRef]
35. Wold, S.; Ruhe, A.; Wold, H.; Dunn, W.J., III. The collinearity problem in linear regression. The partial least squares approach to generalized inverses. *SIAM J. Sci. Stat. Comput.* **1984**, *5*, 735–743. [CrossRef]
36. Wold, S.; Sjöström, M.; Eriksson, L. PLS—Regression: A basic tool of chemometrics. *Chemom. Intell. Lab. Syst.* **2001**, *58*, 109–130. [CrossRef]
37. Asner, G.P.; Martin, R.E.; Knapp, D.E.; Tupayachi, R.; Anderson, C.; Carranza, L.; Martinez, P.; Houcheime, M.; Sinca, F.; Weiss, P. Spectroscopy of canopy chemicals in humid tropical forests. *Remote Sens. Environ.* **2011**, *115*, 3587–3598. [CrossRef]
38. Asner, G.P.; Martin, R.E.; Suhaili, A.B. Sources of canopy chemical and spectral diversity in lowland Bornean forest. *Ecosystems* **2012**, *15*, 504–517. [CrossRef]
39. Gökkaya, K.; Thomas, V.; Noland, T.L.; McCaughey, H.; Morrison, I.; Treitz, P. Prediction of macronutrients at the canopy level using spaceborne imaging spectroscopy and LiDAR data in a mixedwood boreal forest. *Remote Sens.* **2015**, *7*, 9045–9069. [CrossRef]
40. Stein, B.R.; Thomas, V.A.; Lorentz, L.J.; Strahm, B.D. Predicting Macronutrient Concentrations from Loblolly Pine Leaf Reflectance across Local and Regional Scales. *GISci. Remote Sens.* **2014**, *51*, 269–287. [CrossRef]
41. Cleveland, C.C.; Houlton, B.Z.; Smith, W.K.; Marklein, A.R.; Reed, S.C.; Parton, W.; Grosso, S.J.D.; Running, S.W. Patterns of new versus recycled primary production in the terrestrial biosphere. *Proc. Natl. Acad. Sci. USA* **2013**, *110*, 12733–12737. [CrossRef] [PubMed]
42. Grace, J.; Malhi, Y.; Meir, P. Productivity of tropical rain forests. In *Terrestrial Global Productivity: Past, Present and Future*; Mooney, H.A., Roy, J., Saugier, B., Eds.; Academic Press: London, UK, 2001; pp. 401–426.

43. Malhi, Y.; Grace, J. Tropical forests and atmospheric carbon dioxide. *Trends Ecol. Evol.* **2000**, *15*, 332–337. [CrossRef]
44. Brienen, R.J.W.; Phillips, O.L.; Feldpausch, T.R.; Gloor, E.; Baker, T.R.; Lloyd, J.; Lopez-Gonzalez, G.; Monteagudo-Mendoza, A.; Malhi, Y.; Lewis, S.L.; et al. Long-term decline of the Amazon carbon sink. *Nature* **2015**, *519*, 344–348. [CrossRef] [PubMed]
45. Cleveland, C.C.; Taylor, P.; Chadwick, K.D.; Dahlin, K.; Doughty, C.E.; Malhi, Y.; Smith, W.K.; Sullivan, B.W.; Wieder, W.R.; Townsend, A.R. A comparison of plot-based satellite and Earth system model estimates of tropical forest net primary production. *Glob. Biogeochem. Cycles* **2015**, *29*, 626–644. [CrossRef]
46. Huang, C.; Asner, G.P. Applications of remote sensing to alien invasive plant studies. *Sensors* **2009**, *9*, 4869–4889. [CrossRef] [PubMed]
47. Cho, M.A.; Mathieu, R.; Asner, G.P.; Naidoo, L.; van Aardt, J.; Ramoelo, A.; Debba, P.; Wessels, K.; Main, R.; Smit, I.P.; et al. Mapping tree species composition in south african savannas using an integrated airborne spectral and LiDAR system. *Remote Sens. Environ.* **2012**, *125*, 214–226. [CrossRef]
48. Asner, G.P.; Knapp, D.E.; Anderson, C.B.; Martin, R.E.; Vaughn, N. Large-scale climatic and geophysical controls on the leaf economics spectrum. *Proc. Natl. Acad. Sci. USA* **2016**, *113*, 4043–4051. [CrossRef] [PubMed]
49. Pajares, G. Overview and current status of remote sensing applications based on unmanned aerial vehicles (UAVs). *Photogramm. Eng. Remote Sens.* **2015**, *81*, 281–330. [CrossRef]
50. Asner, G.P.; Jones, M.O.; Martin, R.E.; Knapp, D.E.; Hughes, R.F. Remote sensing of native and invasive species in Hawaiian forests. *Remote Sens. Environ.* **2008**, *112*, 1912–1926. [CrossRef]
51. Asner, G.P.; Martin, R.E.; Knapp, D.E.; Tupayachi, R.; Anderson, C.B.; Sinca, F.; Vaughn, N.R.; Llactayo, W. Airborne laser-guided imaging spectroscopy to map forest trait diversity and guide conservation. *Science* **2017**, *355*, 385–389. [CrossRef] [PubMed]
52. Moore, S.; Adu-Bredu, S.; Duah-Gyamfi, A.; Addo-Danso, S.; Ibrahim, F.; Mbou, A.T.; de Grandcourt, A.; Valentini, R.; Nicolini, G.; Djagbletey, G.; et al. Forest biomass, productivity and carbon cycling along a rainfall gradient in West Africa. *Glob. Chang. Biol.* **2017**, *24*, 496–510. [CrossRef] [PubMed]
53. Tiessen, H.; Hauffe, H.; Mermut, A.R. Deposition of Harmattan dust and its influence on base saturation of soils in northern Ghana. *Geoderma* **1991**, *49*, 285–299. [CrossRef]
54. Gvozdevaite, A.; Oliveras, I.; Domingues, T.F.; Peprah, T.; Boakye, M.; Afriyie, L.; da Silva, K.P.; de Farias, J.; de Oliveira, E.A.; Farias, C.C.A.; et al. Leaf-level photosynthetic capacity dynamics in relation to soil and foliar nutrients along forest-savanna ecotones in Ghana and Brazil. *Plant Cell Environ.* **2018**, in press.
55. Suomalainen, J.; Anders, N.; Iqbal, S.; Roerink, G.; Franke, J.; Wenting, P.; Hünniger, D.; Bartholomeus, H.; Becker, R.; Kooistra, L. A lightweight hyperspectral mapping system and photogrammetric processing chain for unmanned aerial vehicles. *Remote Sens.* **2014**, *6*, 11013–11030. [CrossRef]
56. Smith, G.M.; Milton, E.J. The use of the empirical line method to calibrate remotely sensed data to reflectance. *Int. J. Remote. Sens.* **1999**, *20*, 2653–2662. [CrossRef]
57. Weier, J.; Herring, D. Measuring Vegetation (NDVI and EVI). NASA Earth Observatory, 2000. Available online: https://earthobservatory.nasa.gov/Features/MeasuringVegetation/ (accessed on 16 September 2018).
58. Zhang, L.; Sun, X.; Wu, T.; Zhang, H. An analysis of shadow effects on spectral vegetation indexes using a ground-based imaging spectrometer. *IEEE Geosci. Remote Sens. Lett.* **2015**, *12*, 2188–2192. [CrossRef]
59. Dalponte, M.; Ene, L.T.; Marconcini, M.; Gobakken, T.; Næsset, E. Semi-supervised SVM for individual tree crown species classification. *ISPR.S J. Photogram. Remote Sens.* **2015**, *110*, 77–87. [CrossRef]
60. Leckie, D.; Gougeon, F.; Hill, D.; Quinn, R.; Armstrong, L.; Shreenan, R. Combined high-density lidar and multispectral imagery for individual tree crown analysis. *Can. J. For. Res.* **2003**, *29*, 633–649. [CrossRef]
61. Clark, M.L.; Roberts, D.A.; Clark, D.B. Hyperspectral discrimination of tropical rain forest tree species at leaf to crown scales. *Remote Sens. Environ.* **2005**, *96*, 375–398. [CrossRef]
62. Haaland, D.M.; Thomas, E.V. Partial least-squares methods for spectral analyses. 1. relation to other quantitative calibration methods and the extraction of qualitative information. *Anal. Chem.* **1988**, *60*, 1193–1202. [CrossRef]
63. StatSoft, Inc. *Electronic Statistics Textbook*; StatSoft: Tulsa, OK, USA, 2013; Available online: http://www.statsoft.com/textbook/ (accessed on 16 September 2018).
64. Asner, G.P.; Martin, R.E.; Anderson, C.B.; Kryston, K.; Vaughn, N.; Knapp, D.E.; Bentley, L.P.; Shenkin, A.; Salinas, N.; Sinca, F.; et al. Scale dependence of canopy trait distributions along a tropical forest elevation gradient. *New Phytol.* **2016**, *214*, 973–988. [CrossRef] [PubMed]

65. Asner, G.P.; Martin, R.E. Canopy phylogenetic, chemical and spectral assembly in a lowland amazonian forest. *New Phytol.* **2011**, *189*, 999–1012. [CrossRef] [PubMed]
66. Asner, G.P.; Martin, R.E.; Tupayachi, R.; Anderson, C.B.; Sinca, F.; Loreli Carranza-Jiménez and Martinez, P. Amazonian functional diversity from forest canopy chemical assembly. *Proc. Natl. Acad. Sci. USA* **2014**, *111*, 5604. [CrossRef] [PubMed]
67. Bakker, M.; Carreno-Rocabado, G.; Poorter, L. Leaf economics traits predict litter decomposition of tropical plants and differ among land use types. *Funct. Ecol.* **2011**, *25*, 473–483. [CrossRef]
68. Hättenschwiler, S.; Coq, S.; Barantal, S.; Handa, I.T. Leaf traits and decomposition in tropical rainforests: Revisiting some commonly held views and towards a new hypothesis. *New Phytol.* **2011**, *189*, 950. [CrossRef] [PubMed]
69. Ordoñez, J.C.; Van Bodegom, P.M.; Witte, J.M.; Wright, I.J.; Reich, P.B.; Aerts, R. A global study of relationships between leaf traits, climate and soil measures of nutrient fertility. *Glob. Ecol. Biogeogr.* **2009**, *18*, 137–149. [CrossRef]
70. Chavana-Bryant, C.; Malhi, Y.; Wu, J.; Asner, G.P.; Anastasiou, A.; Enquist, B.J.; Caravasi, E.G.C.; Doughty, C.E.; Saleska, S.R.; Martin, R.E.; et al. Leaf aging of Amazonian canopy trees as revealed by spectral and physiochemical measurements. *New Phytol.* **2017**, *214*, 1049–1063. [CrossRef] [PubMed]
71. Gitelson, A.A.; Gritz, Y.; Merzlyak, M.N. Relationships between leaf chlorophyll content and spectral reflectance and algorithms for non-destructive chlorophyll assessment in higher plant leaves. *J. Plant Physiol.* **2003**, *160*, 271–282. [CrossRef] [PubMed]
72. West, J.S.; Bravo, C.; Oberti, R.; Lemaire, D.; Moshou, D.; McCartney, H.A. The potential for optical canopy measurements for targeted control of field crop diseases. *Annu. Rev. Phytopathol.* **2003**, *41*, 593–614. [CrossRef] [PubMed]
73. Wu, J.; Chavana-Bryant, C.; Prohaska, N.; Serbin, S.P.; Guan, K.; Albert, L.P.; Yang, X.; Leeuwen, W.J.D.; Garnello, A.J.; Martins, G.; et al. Convergence in relationships between leaf traits, spectra and age across diverse canopy environments and two contrasting tropical forests. *New Phytol.* **2017**, *214*, 1033–1048. [CrossRef] [PubMed]
74. Lee, D.W.; Bone, R.A.; Tarsis, S.L.; Storch, D. Correlates of leaf optical properties in tropical forest sun and extreme-shade plants. *Am. J. Bot.* **1990**, 370–380. [CrossRef]
75. Ellsworth, D.; Reich, P. Canopy structure and vertical patterns of photosynthesis and related leaf traits in a deciduous forest. *Oecologia* **1993**, *96*, 169–178. [CrossRef] [PubMed]
76. Garnier, E.; Laurent, G.; Bellmann, A.; Debain, S.; Berthelier, P.; Ducout, B.; Roumet, C.; Navas, M.L. Consistency of species ranking based on functional leaf traits. *New Phytol.* **2001**, *152*, 69–83. [CrossRef]
77. Riipi, M.; Haukioja, E.; Lempa, K.; Ossipov, V.; Ossipova, S.; Pihlaja, K. Ranking of individual mountain birch trees in terms of leaf chemistry: Seasonal and annual variation. *Chemoecology* **2004**, *14*, 31–43. [CrossRef]
78. Gotsch, S.G.; Powers, J.S.; Lerdau, M.T. Leaf traits and water relations of 12 evergreen species in Costa Rican wet and dry forests: Patterns of intra-specific variation across forests and seasons. *Plant Ecol.* **2010**, *211*, 133–146. [CrossRef]
79. Ebbers, M.; Wallis, I.; Dury, S.; Floyd, R.; Foley, W. Spectrometric prediction of secondary metabolites and nitrogen in fresh eucalyptus foliage: Towards remote sensing of the nutritional quality of foliage for leaf-eating marsupials. *Aust. J. Bot.* **2002**, *50*, 761–768. [CrossRef]
80. Kokaly, R.F.; Asner, G.P.; Ollinger, S.V.; Martin, M.E.; Wessman, C.A. Characterizing canopy biochemistry from imaging spectroscopy and its application to ecosystem studies. *Remote Sens. Environ.* **2009**, *113*, S78–S91. [CrossRef]
81. Skidmore, A.K.; Ferwerda, J.G.; Mutanga, O.; Van Wieren, S.E.; Peel, M.; Grant, R.C.; Prins, H.H.; Balcik, F.B.; Venus, V. Forage quality of savannas—Simultaneously mapping foliar protein and polyphenols for trees and grass using hyperspectral imagery. *Remote Sens. Environ.* **2010**, *114*, 64–72. [CrossRef]
82. Blaaberg, S.; Løke, T.; Baarstad, I.; Fridman, A.; Koirala, P. HySpex ODIN-1024: A new high-resolution airborne HSI system. *Infrared Technol. Appl. XL* **2014**, *90700*. [CrossRef]
83. Asner, G.P.; Knapp, D.E.; Boardman, J.; Green, R.O.; Kennedy-Bowdoin, T.; Eastwood, M.; Martin, R.E.; Anderson, C.; Field, C.B. Carnegie Airborne Observatory-2: Increasing science data dimensionality via high-fidelity multi-sensor fusion. *Remote Sens. Environ.* **2012**, *124*, 454–465. [CrossRef]

84. Verrelst, J.; Malenovský, Z.; Van der Tol, C.; Camps-Valls, G.; Gastellu-Etchegorry, J.-P.; Lewis, P.; North, P.; Moreno, J. Quantifying Vegetation Biophysical Variables from Imaging Spectroscopy Data: A Review on Retrieval Methods. *Surv. Geophys.* **2018**, 1–41. [CrossRef]
85. Marvin, D.C.; Asner, G.P.; Knapp, D.E.; Anderson, C.B.; Martin, R.E.; Sinca, F.; Tupayachi, R. Amazonian landscapes and the bias in field studies of forest structure and biomass. *Proc. Natl. Acad. Sci. USA* **2014**, *111*, 5224–5232. [CrossRef] [PubMed]
86. Hidaka, A.; Kitayama, K. Allocation of foliar phosphorus fractions and leaf traits of tropical tree species in response to decreased soil phosphorus availability on Mount Kinabalu, Borneo. *J. Ecol.* **2011**, *99*, 849–857. [CrossRef]
87. Asner, G.P.; Martin, R.E.; Carranza-Jiménez, L.; Sinca, F.; Tupayachi, R.; Anderson, C.B.; Martinez, P. Functional and biological diversity of foliar spectra in tree canopies throughout the Andes to Amazon region. *New Phytol.* **2014**, *204*, 127–139. [CrossRef] [PubMed]
88. Santiago, L.S.; Kitajima, K.; Wright, S.J.; Mulkey, S.S. Coordinated changes in photosynthesis, water relations and leaf nutritional traits of canopy trees along a precipitation gradient in lowland tropical forest. *Oecologia* **2004**, *139*, 495–502. [CrossRef] [PubMed]
89. Santiago, L.; Goldstein, G.; Meinzer, F.; Fisher, J.; Machado, K.; Woodruff, D.; Jones, T. Leaf photosynthetic traits scale with hydraulic conductivity and wood density in Panamanian forest canopy trees. *Oecologia* **2004**, *140*, 543–550. [CrossRef] [PubMed]
90. Maharjan, S.K.; Poorter, L.; Holmgren, M.; Bongers, F.; Wieringa, J.J.; Hawthorne, W.D. Plant functional traits and the distribution of West African rain forest trees along the rainfall gradient. *Biotropica* **2011**, *43*, 552–561. [CrossRef]
91. Givnish, T.J. Altitudinal gradients in tropical forest composition, structure, and diversity in the sierra de manantlán. *J. Ecol.* **1998**, *86*, 999–1020. [CrossRef]
92. Cunningham, S.A.; Summerhayes, B.; Westoby, M. Evolutionary divergences in leaf structure and chemistry, comparing rainfall and soil nutrient gradients. *Ecol. Monogr.* **1999**, *69*, 569–588. [CrossRef]
93. Malhi, Y.; Doughty, C.E.; Goldsmith, G.R.; Metcalfe, D.B.; Girardin, C.A.; Marthews, T.R.; del Aguila-Pasquel, J.; Aragão, L.E.; Araujo-Murakami, A.; Brando, P.; et al. The linkages between photosynthesis, productivity, growth and biomass in lowland Amazonian forests. *Glob. Chang. Biol.* **2015**, *21*, 2283–2295. [CrossRef] [PubMed]
94. Meir, P.; Grace, J.; Miranda, A.C. Leaf respiration in two tropical rainforests: Constraints on physiology by phosphorus, nitrogen and temperature. *Funct. Ecol.* **2001**, *15*, 378–387. [CrossRef]
95. Weg, V.D.; Meir, P.; Grace, J.; Atkin, O.K. Altitudinal variation in leaf mass per unit area, leaf tissue density and foliar nitrogen and phosphorus content along an Amazon- Andes gradient in Peru. *Plant Ecol. Divers.* **2009**, *2*, 243–254. [CrossRef]
96. Li, L.; McCormack, M.L.; Ma, C.; Kong, D.; Zhang, Q.; Chen, X.; Zeng, H.; Niinemets, U.; Guo, D. Leaf economics and hydraulic traits are decoupled in five species-rich tropical-subtropical forests. *Ecol. Lett.* **2015**, *18*, 899–906. [CrossRef] [PubMed]
97. De la Riva, E.G.; Olmo, M.; Poorter, H.; Ubera, J.L.; Villar, R. Leaf mass per area (LMA) and its relationship with leaf structure and anatomy in 34 Mediterranean woody species along a water availability gradient. *PLoS ONE* **2016**, *11*, e0148788. [CrossRef] [PubMed]
98. Porder, S.; Asner, G.P.; Vitousek, P.M. Ground-based and remotely sensed nutrient availability across a tropical landscape. *Proc. Natl. Acad. Sci. USA* **2005**, *102*, 10909–10912. [CrossRef] [PubMed]
99. Demarty, M.; Morvan, C.; Thellier, M. Calcium and the cell wall. *Plant Cell Environ.* **1984**, *7*, 441–448. [CrossRef]
100. Stuffler, T.; Kaufmann, C.; Hofer, S.; Förster, K.P.; Schreier, G.; Mueller, A.; Eckardt, A.; Bach, H.; Penné, B.; Benz, U.; et al. The EnMAP hyperspectral imager—An advanced optical payload for future applications in Earth observation programmes. *Acta Astronaut.* **2007**, *61*, 115–120. [CrossRef]
101. Moreno, J.; Asner, G.P.; Bach, H.; Belenguer, T.; Bell, A.; Buschmann, C.; Calera, A.; Calpe, J.; Campbell, P.; Cecchi, G.; et al. Fluorescence explorer (FLEX): An optimised payload to map vegetation photosynthesis from space. In Proceedings of the AIAA 57th International Astronautical Congress, Valencia, Spain, 2–6 October 2006; Volume 3, pp. 2065–2074. [CrossRef]
102. Iwasaki, A.; Ohgi, N.; Tanii, J.; Kawashima, T.; Inada, H. Hyperspectral Imager Suite (HISUI)-Japanese Hyper-Multi Spectral Radiometer. In Proceedings of the IEEE International Geoscience and Remote Sensing Symposium, Vancouver, BC, Canada, 24–29 July 2011. [CrossRef]

103. Lee, C.M.; Cable, M.L.; Hook, S.J.; Green, R.O.; Ustin, S.L.; Mandl, D.J.; Middleton, E.M. An introduction to the NASA Hyperspectral InfraRed Imager (HyspIRI) mission and preparatory activities. *Remote Sens. Environ.* **2015**, *167*, 6–19. [CrossRef]
104. Pignatti, S.; Palombo, A.; Pascucci, S.; Romano, F.; Santini, F.; Tiziana, S.; Umberto, A.; Vincenzo, C.; Acito, N.; Marco, D.; et al. The PRISMA hyperspectral mission: Science activities and opportunities for agriculture and land monitoring. In Proceedings of the IEEE International Geoscience and Remote Sensing Symposium (IGARSS), Melbourne, Australia, 21–26 July 2013. [CrossRef]
105. Natale, V.G.; Kafri, A.; Tidhar, G.A.; Chen, M.; Feingersh, T.; Sagi, E.; Cisbani, A.; Baroni, M.; Labate, D.; Nadler, R.; et al. SHALOM—Space-borne hyperspectral applicative land and ocean mission. In Proceedings of the 5th Workshop on Hyperspectral Image and Signal Processing: Evolution in Remote Sensing (WHISPERS), Gainesville, FL, USA, 26–28 June 2013. [CrossRef]
106. Scheiter, S.; Langan, L.; Higgins, S.I. Next-generation dynamic global vegetation models: Learning from community ecology. *New Phytol.* **2013**, *198*, 957–969. [CrossRef] [PubMed]